Structure and mechanism of mitochondrial proton-translocating transhydrogenase

Domen Kampjut and Leonid Sazanov*

Proton-translocating transhydrogenase (NNT), found in the plasma membranes of bacteria and in the inner mitochondrial membranes, catalyses the proton translocation-coupled transhydrogenation NADH + $NADP^+$ + H^+_{out} <-> NAD^+ + NADPH + H^+_{in}. Its physiological function is the generation of NADPH for anabolic reactions and oxidative status regulation, as well as potentially fine-tuning the Krebs cycle[1,2]. NNT deficiency causes familial glucocorticoid deficiency in humans and type II diabetes-like abnormalities in mice (common strain C57BL/6J has dysfunctional transhydrogenase)[3,4]. The catalytic mechanism was proposed to involve a remarkable ~180° rotation of the entire NADP(H)-binding domain that alternately participates in hydride transfer and proton channel gating but the details of this process remained obscure due to the lack of the high-resolution structures of intact NNT[5,6]. Here we report the first atomic structure of intact mammalian transhydrogenase, solved by cryo-EM in different conformational states. We show how the NADP(H)-binding domain opens the proton channel to the opposite sides of the membrane and provide structures of these two states. We also describe the catalytically important interfaces and linkers between the membrane and the soluble domains and their roles in nucleotide exchange. These structures allow us to propose a revised and detailed mechanism for a unique coupling process in transhydrogenase that is consistent with a large body of previous biochemical work. Results presented here are relevant for the development of currently unavailable NNT inhibitors with therapeutic potential in ischaemia reperfusion injury, metabolic syndrome and some cancers[7–9].

Main text

Transhydrogenase always exists as a homodimer. Each monomer is composed of three domains, NAD(H)-binding dI, transmembrane dII and NADP(H)-binding dIII, split between one, two or three polypeptides (Fig. 1a, Extended Data Fig. 1). Structures of isolated domains and dI_2dIII complexes from several species were solved in native, reduced or oxidised states, however, they failed to explain the unique mechanism of NNT which requires coordination of all the domains in the dimer[10–14]. The only intact architecture of NNT was determined at low resolution (6.9 Å) for the *T. thermophilus* enzyme in the presence of $NADP^+$[5]. It showed that NNT is an asymmetric dimer, with one dIII being "face-up" (presenting NADP(H) to dI for hydride transfer) and the other dIII being "face-down" (with NADP(H) site facing dII) (Fig. 1b)[5]. This led to a proposal of a unique "division of labour" mechanism in which dIII rotates ~180^0 and alternatively functions in proton translocation (face-down) and hydride transfer (face-up)[6]. While being consistent with the *T. thermophilus* architecture and most of the previous biochemical work, in the absence of detailed structural information the mechanism was largely speculative and it failed to account for the different effects of $NADP^+$/NADPH on the conformation of NNT[15,16].

To define the mechanism, we solved structures of a stable and active preparation of ovine NNT at pH 7.4 in the apo, $NADP^+$-bound and NADPH-bound forms at up to 2.9 Å resolution using cryo-EM (Extended Data Fig. 2-4). The only observed 3D class of particles in the apo-NNT dataset adopted an unexpected and previously unobserved "double face-down" conformation with both dIII domains tightly attached

to dII in the "face-down" orientation (Fig. 1a). In the $NADP^+$ dataset the main class showed a similar conformation, but with improved resolution, possibly due to the stabilising effects of the bound nucleotide (Fig. 1c and 2a, Extended Data Fig. 3 and 5). $NADP^+$ dataset also resulted in the structure of the less populated class ("single face-down", Fig. 1b) in which one dIII is detached from dII, dI_2 is more tilted and, importantly, the proton channel has different conformations in the two monomers, as discussed below (Extended Data Fig. 6). Excellent EM maps resulted in high quality full atomic models of mammalian NNT (Extended Data Fig. 5-6, Extended Data Table 1). Incubating NNT with NADPH induced global conformational changes, as predicted[15,16], and we did not observe any "double face-down" class (Fig. 2a, Extended Data Fig. 4a). Only ~11 % of particles had one dIII weakly bound to dII and the rest of the particles corresponded to many different "double-detached" classes with both dIII domains detached and tethered only by a dII-dIII linker, which allowed striking tilting of dI_2 in all directions (Fig. 2). We conclude that in the mammalian enzyme, $NADP^+$ and NADPH on their own promote dIII detachment to various degrees but do not lead to a stable dI-dIII (face-up) interface formation.

Some novel features of the structure, such as dI-dII linker, and other additional results are described in the Supplementary Discussion. The mammalian-specific helices TM1 and TM5 form an unexpected extended dII dimer interface, possibly stabilising mammalian NNT (Fig. 3a). The core fold of dII is conserved between *T. thermophilus* and ovine. The likely proton translocation pathway, as proposed earlier, is formed by TM3-4, TM9-10, and TM13-14, arranged in a hexagram[5,17,18]. We observed two conformations of the proton channel, depending on the attachment of the dIII domain, which inserts the helix 4 (residues 929-937) and the $NADP^+$-

coordinating loop (residues 920-927) deeply between the key TM helices 3, 9 and 13, pushing them apart (Fig. 4a,b). Analysis of the proton channel in the dIII-attached state starting from the N-side (bacterial cytoplasm or mitochondrial matrix) indicates a narrow block followed by a group of conserved polar residues (His664, Asn796 and Asn489), a dry hydrophobic stretch and a cluster of negatively charged residues at the exit, appropriate for proton "gathering" from the P-side in forward reaction (Fig. 3b,c, Extended Data Fig. 6g). Strikingly, secondary structures of helices TM3 and TM9 are distorted around this region, signifying the conformational flexibility needed for the proton translocation (Fig. 3b).

dIII detachment from dII induces a significant shift of the loops CL6/CL7, helix CL8 and the matrix-facing sides of TM9, 10, 11, 13 and 14 towards the centre of the dII, with up to 3.5 Å displacements (Fig. 4a). This results in a more compact packing of the helices making dIII-detached dII much more similar to the *T. thermophilus* dII (also detached from dIII) than dIII-attached dII (Extended data Fig. 7a,b). With dIII detached, the proton channel adopts a more closed conformation from the P-side (Extended data Fig. 7f,g). Dramatically, H664 flips "down" (towards P-side) and S799 "up", in line with the MD predictions (Fig 4a, Extended Data Fig. 7c)[17]. H664 becomes more accessible for protonation from the matrix side, both due to the re-arrangements in the channel and, importantly, the removal of the dIII-NADP(H) "plug", exposing the dII surface to the solvent (Fig. 3). Modelling of water molecules is consistent with this conclusion: in the dIII-attached dII one water molecule is bound above and one below the H664-N489-N796 ring while in the dIII-detached state, the P-side water molecule disappears and the S799 flips "downwards" (Extended Data

Fig. 7d). Cryo-EM density of the highly coordinated P-side water molecule is visible in our 2.9 Å map (Extended Data Fig. 7e).

The conformation of dIII bound to dII differs from crystal structures of isolated dIII at the interface-forming sites and in the nucleotide binding pocket (Fig. 4b, Extended Data Fig. 8a)[10,11,14]. Loop E (residues 1002-1010) is a transhydrogenase-specific element that "occludes" the nucleotide in isolated dIII, preventing its exchange with the solution[10,12]. This loop is displaced by the dII CL7 and has only very weak density in our "double face-down" $NADP^+$ structure, allowing $NADP^+$ to insert deeply into the proton channel. In the apo-NNT structure, loop E is completely disordered allowing free exchange of nucleotide (Extended data Fig. 8b,c). dII binding also induces some opening around the ribose diphosphate, i.e. breaking of the R925-Y890 stacking interactions and the R925 bonds with the diphosphate that have not been observed in any dIII or dI_2dIII crystal structures (Fig 4c)[10,12]. In apo-NNT, this opening is even more pronounced with R925 being rotated outwards (Extended Data Fig. 8c). We conclude that the $NADP^+$ molecule is partially occluded in the face-down binding site, but less so than in the detached dIII.

We can now revise the catalytic mechanism of transhydrogenase, involving dIII flipping as proposed earlier[6], on the basis of our observations and previous functional and mutagenesis results (Extended Data Fig. 9a, Supplementary Tables 1-3), summarised in the following principal considerations.

It has been well established from previous work that: a) dI remains open to nucleotide exchange throughout the reaction cycle as confirmed by high rates of

125 binding of NAD(H) to dI during the catalytic cycle[19,20]. b) The dI-dIII interface is
126 transient, hydride transfer is fast and does not limit the reaction[21]. c) When dIII is
127 detached, bound NADP(H) is occluded, as shown by decreased K_d for NADP(H) in
128 isolated dIII (~10^{-9} M) compared to intact enzyme (~10^{-6} M), copurification of bound
129 nucleotide with isolated dIII and well-ordered and closed loop E in dIII
130 structures[10,12,22,23]. H664 and R544 mutations which lead to dIII detachment also lead
131 to co-purification with NADP(H)[18,24].
132
133 The following principle was speculatively proposed earlier[6] and is now validated
134 by our structures: d) The formation of the dII-dIII interface is necessary for nucleotide
135 exchange, as shown by our structures demonstrating loop E opening (Extended Data
136 Fig. 8). It is further validated by R544 mutants which disrupt the dII-dIII interface[24].
137
138 Crucial new insights from the structural data presented here are: e) Apo-dIII is
139 attached to dII and can detach only when bound to NADP(H) (Fig. 2a). f) The proton
140 channel is open only to the N-side when dIII is detached and only to the P-side when
141 dIII is attached (Fig. 4, Extended Data Fig. 7). g) The dIII-NADP(H) detachment
142 from dII depends on the protonation state of the key histidine in the proton channel
143 (H664 in ovine). dIII-$NADP^+$ is detached from protonated $H664^+$ but is attached to
144 the neutral H664. Vice versa, dIII-NADPH is detached from H664 and is attached to
145 $H664^+$. In other words, dIII-NADP(H) attachment modifies H664 pK_a: bound
146 NADPH promotes its protonation and $NADP^+$ de-protonation. This pattern is
147 consistent with the direct electrostatic interaction between H664 and the charged
148 nicotinamide ring (positive in $NADP^+$ and negative in NADPH) separated only by
149 about 13 Å (Fig. 3e), much closer than 19 Å predicted previously[5]. The pK_a of His664

150 was experimentally estimated to be ~5.5[25], which is consistent with PROPKA
151 calculations on our structures (suggesting pK_a ~5). Since our datasets were collected
152 at pH 7.4, when H664 is mostly de-protonated, we observed mostly attached dIII-
153 $NADP^+$ and mostly detached dIII-NADPH, consistent with this proposal. dIII
154 detachment from dII in the presence of $NADP^+$ and $H664^+$ is also validated by low
155 pH-stimulation of $NADP^+$-dependent cyclic reaction (hydride transfer from NADH to
156 NAD^+ via occluded $NADP^+$)[25,26]. Cyclic reaction cannot inform us on specific
157 NADPH effects as the main species in the NADPH-initiated cycle is still the occluded
158 dIII-$NADP^+$[26]. However, NADPH-stimulated dIII detachment at neutral-high pH has
159 been demonstrated experimentally by stimulated trypsinolysis in the presence of
160 NADPH (but not NADH/NAD^+)[15]. We analysed the full pH dependence of
161 trypsinolysis in the presence of all substrates and showed that NADPH stimulates
162 trypsinolysis with increasing pH, while $NADP^+$ stimulates it with decreasing pH
163 (Extended Data Fig. 2e), validating the predicted H664-NADP(H) interactions.
164
165 On the basis of these principles we propose a robust and elegant mechanism
166 which explains the full reversibility of NNT, pH dependencies of reverse and cyclic
167 reactions, effects of $NADP^+$ and NADPH on the NNT conformation and is validated
168 by the phenotypes of various mutants, particularly within the proton translocation
169 pathway, E loop and dII-dIII interface (Fig. 5, Supplementary Video 1). Proton
170 translocation and nucleotide exchange are tightly coupled by direct interactions
171 between H664 and NADP(H): attachment/detachment of NADP(H)-bound dIII is
172 strictly dependent on the protonation state of H664 and opens the proton channel to
173 the opposite sides of the membrane. “Slipping”, or uncoupling, is prevented because
174 proton translocation cannot happen without nucleotide exchange. The forward

175 reaction occurs under conditions with high pmf and excess of $NADP^+$. With dIII
176 detached, H664 is unprotonated as it is exposed to the matrix with its relatively high
177 pH (step 1, Fig. 5). After hydride transfer, dIII-NADPH swivels down and attaches to
178 dII-H664, opening it to the P-side (step 2). This allows H664 protonation from the P-
179 side, where pH is lower (and His pK_a is shifted higher due to interaction with
180 NADPH). Nucleotide exchange follows, due to $NADP^+$ excess and opened dIII (step
181 3). dIII-$NADP^+$ detaches from dII-$H664^+$, which opens dII to the N-side where $H664^+$
182 is de-protonated (step 4). dIII-$NADP^+$ associates with dI, allowing for hydride transfer
183 (back to step 1). All the steps can be easily reversed in the appropriate conditions
184 (high NADPH and low pmf), giving rise to the reverse reaction (Extended Data Fig.
185 9b, Supplementary Discussion).
186
187 This mechanism implies anti-phase action of two monomers, or "division of
188 labour" as suggested previously[6], which is absolutely necessary for bacterial enzymes
189 without dI-dII linker, where one dIII has to be attached to dI_2 at all times to prevent
190 the loss of dI_2. Mammalian NNT also demonstrates half-of-sites inhibition,
191 catalytically inactive monomeric dI and negative cooperativity of NAD(H) and
192 NADP(H) sites between monomers, strongly suggesting anti-phase mechanism[27–29].
193 The presence of dI-dII linker could make a strict anti-phase action less of a
194 requirement for the mammalian enzyme, but such action would avoid steric clashes
195 between independently functioning dIIIs and the swivelling "up" of one dIII is the
196 best explanation for the initiation of the detachment, after hydride transfer, of the
197 other dIII from dI_2. The dI-dII linker could also contribute towards higher efficiency
198 of the mammalian enzyme, as the dI-dIII interface can be weaker and allow for faster
199 turnover. Biochemical data confirms that dI-dIII interaction in bacteria is much

200 stronger than in mammals[20,30]. The existence of a unique auto-inhibited "double face-
201 down" conformation in mammalian NNT could be important for its additional
202 regulation. Further data will be required to determine the significance of the anti-
203 phase action in NNT as well as to test all the implications of the proposed mechanism.
204

205 **References**

206 1. Jackson, J. B. A review of the binding-change mechanism for proton-
207 translocating transhydrogenase. *Biochim. Biophys. Acta - Bioenerg.* **1817**,
208 1839–1846 (2012).
209 2. Sazanov, L. A. & Jackson, J. B. Proton-translocating transhydrogenase and
210 NAD- and NADP-linked isocitrate dehydrogenases operate in a substrate cycle
211 which contributes to fine regulation of the tricarboxylic acid cycle activity in
212 mitochondria. *FEBS Lett.* **344**, 109–116 (1994).
213 3. Meimaridou, E. *et al.* Mutations in NNT encoding nicotinamide nucleotide
214 transhydrogenase cause familial glucocorticoid deficiency. *Nat. Genet.* **44**,
215 740–2 (2012).
216 4. Toye, A. A. *et al.* A genetic and physiological study of impaired glucose
217 homeostasis control in C57BL/6J mice. *Diabetologia* **48**, 675–686 (2005).
218 5. Leung, J. H. *et al.* Structural biology. Division of labor in transhydrogenase by
219 alternating proton translocation and hydride transfer. *Science* **347**, 178–81
220 (2015).
221 6. Jackson, J. B., Leung, J. H., Stout, C. D., Schurig-Briccio, L. A. & Gennis, R.
222 B. Review and Hypothesis. New insights into the reaction mechanism of
223 transhydrogenase: Swivelling the dIII component may gate the proton channel.
224 *FEBS Letters* **589**, 2027–2033 (2015).
225 7. Li, S. *et al.* Nicotinamide nucleotide transhydrogenase-mediated redox
226 homeostasis promotes tumor growth and metastasis in gastric cancer. *Redox*
227 *Biol.* **18**, 246–255 (2018).
228 8. Santos, L. R. B. *et al.* NNT reverse mode of operation mediates glucose control
229 of mitochondrial NADPH and glutathione redox state in mouse pancreatic β-

cells. *Mol. Metab.* **6**, 535–547 (2017).

9. Nickel, A. G. *et al.* Reversal of Mitochondrial Transhydrogenase Causes Oxidative Stress in Heart Failure. *Cell Metab.* **22**, 472–484 (2015).

10. Prasad, G. S., Sridhar, V., Yamaguchi, M., Hatefi, Y. & Stout, C. D. Crystal structure of transhydrogenase domain III at 1.2 A resolution. *Nat. Struct. Biol.* **6**, 1126–31 (1999).

11. Cotton, N. P. J., White, S. A., Peake, S. J., Mcsweeney, S. & Jackson, J. B. The Crystal Structure of an Asymmetric Complex of the Two Nucleotide Binding Components of Proton-Translocating Transhydrogenase. *Structure* **9**, 165–176 (2001).

12. Sundaresan, V., Yamaguchi, M., Chartron, J. & Stout, C. D. Conformational Change in the NADP(H) Binding Domain of Transhydrogenase Defines Four States. *Biochemistry* **42**, 12143–12153 (2003).

13. Johansson, T. *et al.* X-ray structure of domain I of the proton-pumping membrane protein transhydrogenase from *Escherichia coli*. *J. Mol. Biol.* **352**, 299–312 (2005).

14. Mather, O. C., Singh, A., Van Boxel, G. I., White, S. A. & Jackson, J. B. Active-site conformational changes associated with hydride transfer in proton-translocating transhydrogenase. *Biochemistry* **43**, 10952–10964 (2004).

15. Yamaguchi, M., Wakabayashi, S. & Hatefi, Y. Mitochondrial Energy-Linked Nicotinamide Nucleotide Transhydrogenase: Effect of Substrates on the Sensitivity of the Enzyme to Trypsin and Identification of Tryptic Cleavage Sites. *Biochemistry* **29**, 4136–4143 (1990).

16. Yamaguchi, M. & Hatefi, Y. Mitochondrial nicotinamide nucleotide transhydrogenase: NADPH binding increases and NADP binding decreases the

acidity and susceptibility to modification of cysteine-893. *Biochemistry* **28**, 6050–6 (1989).

17. Padayatti, P. S. *et al.* Critical Role of Water Molecules in Proton Translocation by the Membrane-Bound Transhydrogenase. *Structure* 1–9 (2017).

18. Glavas, N. A., Hou, C. & Bragg, P. D. Involvement of Histidine-91 of the β Subunit in Proton Translocation by the Pyridine Nucleotide Transhydrogenase of *Escherichia coli*. *Biochemistry* **34**, 7694–7702 (1995).

19. Venning, J. D., Peake, S. J., Quirk, P. G. & Jackson, J. B. Stopped-flow reaction kinetics of recombinant components of proton-translocating transhydrogenase with physiological nucleotides. *J. Biol. Chem.* **275**, 19490–7 (2000).

20. Yamaguchi, M. & Hatefi, Y. High cyclic transhydrogenase activity catalyzed by expressed and reconstituted nucleotide-binding domains of *Rhodospirillum rubrum* transhydrogenase. *Biochim. Biophys. Acta - Bioenerg.* **1318**, 225–234 (1997).

21. Venning, J. D., Bizouarn, T., Cotton, N. P. J., Quirk, P. G. & Jackson, J. B. Stopped-flow kinetics of hydride transfer between nucleotides by recombinant domains of proton-translocating transhydrogenase. *Eur. J. Biochem.* **257**, 202–209 (1998).

22. Fjellström, O., Johansson, C. & Rydström, J. Structural and catalytic properties of the expressed and purified NAD(H)- and NADP(H)-binding domains of proton-pumping transhydrogenase from *Escherichia coli*. *Biochemistry* **36**, 11331–11341 (1997).

23. Bizouarn, T., Van Boxel, G. I., Bhakta, T. & Jackson, J. B. Nucleotide binding affinities of the intact proton-translocating transhydrogenase from *Escherichia*

coli. *Biochim. Biophys. Acta - Bioenerg.* **1708**, 404–410 (2005).

24. Glavas, N. A. & Bragg, P. D. The mechanism of hydride transfer between NADH and 3-acetylpyridine adenine dinucleotide by the pyridine nucleotide transhydrogenase of *Escherichia coli*. *Biochim. Biophys. Acta* **1231**, 297–303 (1995).

25. Sazanov, L. A. & Jackson, J. B. Cyclic reactions catalysed by detergent-dispersed and reconstituted transhydrogenase from beef-heart mitochondria; implications for the mechanism of proton translocation. *Biochim. Biophys. Acta* **1231**, 304–312 (1995).

26. Hutton, M., Day, J. M., Bizouarn, T. & Jackson, J. B. Kinetic resolution of the reaction catalysed by proton-translocating transhydrogenase from *Escherichia coli* as revealed by experiments with analogues of the nucleotide substrates. *Eur. J. Biochem.* **219**, 1041–1051 (1994).

27. Phelps, D. C. & Hatefi, Y. Interaction of purified nicotinamidenucleotide transhydrogenase with dicyclohexylcarbodiimide. *Biochemistry* **23**, 4475–4480 (1984).

28. Yamaguchi, M. & Hatefi, Y. Energy-transducing nicotinamide nucleotide transhydrogenase. Nucleotide binding properties of the purified enzyme and proteolytic fragments. *J. Biol. Chem.* **268**, 17871–17877 (1993).

29. Obiozo, U. M. *et al.* Substitution of tyrosine 146 in the dI component of proton-translocating transhydrogenase leads to reversible dissociation of the active dimer into inactive monomers. *J. Biol. Chem.* **282**, 36434–36443 (2007).

30. Fjellstrom, O. *et al.* Catalytic Properties of Hybrid Complexes of the NAD(H)-Binding and NADP(H)-Binding Domains of the Proton-Translocating Transhydrogenases from *Escherichia coli* and *Rhodospirillum rubrum*.

Biochemistry. **38**, 415–422 (1999).

Main Figure Legends

Figure 1. Mammalian transhydrogenase.

a, Schematic representation of the domains, linkers, binding sites and conformation of the mammalian transhydrogenase in the "double face-down" (both dIII attached to dII) conformation (apo and $NADP^+$ datasets). **b**, Other conformations of NNT present in our datasets (one or both dIII detached in the presence of $NADP^+$ and NADPH), the asymmetric conformation in *T. thermophilus* (N.B. the absence of dI-dII linker) and the sterically prohibited double-face-up conformation. **c**, The cryo-EM density of transhydrogenase in the "double face-down" $NADP^+$ state, with two monomers coloured differently. **d**, Atomic model of mammalian NNT with domains coloured as in panel a, and mammalian-specific elements dI-dII linker, TM1 and TM5 highlighted in blue. Bound nucleotides are shown in black.

Figure 2. NADP(H) binding influences the overall conformation of transhyrogenase.

a, Structures and relative abundancies of different conformations of NNT observed in the datasets. "Double face-down" conformation was the only form observed in apo-NNT and the major form in the $NADP^+$ datasets, "single face-down" or "one dIII-detached" conformation was a minor form in $NADP^+$ and NADPH datasets and "double dIII-detached" was a major form in NADPH dataset. **b**, NNT-NADPH particles were analysed using multibody refinement in RELION 3.0 using dI_2 and dII_2 masks which revealed a high degree of tilting of dI_2 domain in all directions, consistent with both dIII being dissociated from the rest of the particle and disrupting the overall solidity of the enzyme. Two bins of particles from the extreme ends of the distribution along two principal components are aligned by dII_2 and the difference in dI_2 tilt is depicted in different shades of yellow and green.

Figure 3. The transmembrane dII domain and the proton translocation pathway in the "double face-down" conformation.

a, Organisation of transmembrane helices in the NNT dimer. The monomer on the left is coloured blue-to-red from N- to C-terminus and the monomer on the right has the inner proton channel-lining TM helices highlighted in magenta and the outer scaffolding helices in pink. The dimer interface consisting of eight helices is significantly larger than the four-helix interface of *T. thermophilus*. **b**, Conserved residues of the proton transfer pathway. Dowser-predicted water molecules are shown as red spheres. The distorted α-helical area is indicated as 3_{10} helix. **c**, Proton translocating pore features a narrow block close to the matrix (N) side and a dry stretch in the middle of the membrane. Four of the predicted water molecules lie within the central pore. **d**, Detailed view of the matrix proton entry site with conserved residues and hydrogen bonding network shown. **e**, Nicotinamide ring is bound 13 Å away from H664 allowing for electrostatic interactions.

Figure 4. dIII attachment changes the conformation of the proton translocation pathway and opens the NADP(H)-binding pocket.

a, Comparison of dII in dIII-associated (cyan) and dissociated (green) states from "single face-down" structure. dIII dissociation results in the tilting of TM helices towards the central axis. Expanded views show rearrangement of the N-side proton entry side in dII. Notably, H664 and S799 flip and the surrounding N489 and N796 change conformations significantly, opening the channel to the N-side when dIII is detached. **b**, The interface between dIII and dII. Helix 4 and loop D, which are conserved transhydrogenase-specific elements flanking the central Rossmann fold, form extensive contacts with the cytoplasmic loops of the dII. Loop E is displaced by dII binding. **c**, NADP(H) binding pocket comparison between ovine dIII-dII and human dIII-$NADP^+$ (PDB 1djl, in grey) reveals breaking of R925 interactions with diphosphate and Y890.

Figure 5. The catalytic mechanism of transhydrogenase

NNT always works as a dimer. Key steps in the mechanism for the monomer in colour are described in the main text. The other monomer (grey) works in the anti-phase fashion. Nucleotide in dIII exists in either occluded (full line) or open state (dashed line). Key check-point in the mechanism is that proton translocation across the membrane cannot proceed to completion without nucleotide exchange in step 3. The dIII-NADP(H) and dII-H664 interactions, ensuring this coupled reaction, can be summarised as follows, with (*) meaning strong interaction and (←→) weak interaction or repulsion:

$NADP^+$ * H $NADP^+$ ←→ H^+

NADPH * H^+ NADPH ←→ H

Methods

Purification of transhydrogenase from ovine mitochondria

All the described procedures were done at 4°C. Mitochondria were purified from fresh ovine heart tissue by differential centrifugation and stored at –80°C according to the Procedure 3 by Smith[31]. On the day of purification, inner mitochondrial membranes were isolated as described for the respiratory complex I purification[32]. Briefly, 10 g of mitochondria were ruptured by homogenisation in 100 mL milliQ water, membranes were separated by 45 min centrifugation at 50000 g and resuspended in 100 mL of buffer M (20 mM HEPES, pH 7.4, 40 mM NaCl, 1 mM EDTA, 10% v/v glycerol, 2 mM DTT and 0.002% PMSF). After another round of resuspension and centrifugation, membranes were resuspended in 50 mL of buffer M. LMNG (10 %) was added dropwise to this suspension to 1 % and after stirring for 45 min, the sample was centrifuged at 50000 g for 45 minutes. The supernatant was filtered with a 0.22 μm filter and loaded onto a 45 mL Q-sepharose HP anion exchange column equilibrated in buffer Q-A (20 mM HEPES pH7.4, 40 mM NaCl, 2 mM EDTA, 10% v/v glycerol, 1 mM DTT, 0.05% LMNG). Proteins were eluted with a 400 mL linear gradient with 0-17% Q-B buffer (Q-A buffer with 1 M NaCl). NNT eluted as a broad peak around 110 mM NaCl and fractions containing significant amounts of NNT based on the activity assay and the SDS-PAGE profile were pooled and dialysed overnight against a 10-fold volume excess of buffer D (20 mM MES, pH 5.8, 2 mM EDTA, 10% v/v glycerol, 1 mM DTT, 0.01% LMNG). This lowered the pH and conductance of the sample below 6 and 2 mS/cm, respectively, and made it suitable for loading onto a 45 mL SP-Sepharose HP cation exchange column equilibrated in buffer SP-A (20 mM MES pH5.8, 10 mM NaCl, 2 mM EDTA, 10% v/v glycerol, 1 mM DTT, 0.025% LMNG). Elution with a 100 mL 0-20% linear

gradient with buffer SP-B (SP-A with 1 M NaCl) gave a sharp elution peak of relatively pure NNT at around 35 mM NaCl (conductance 4 mS/cm). Fractions containing NNT were concentrated to 4 mg/mL using a 100 kDa cut-off concentrator and stored at 30% glycerol under liquid nitrogen. On the day of a cryo-EM grid preparation, a sample of NNT was thawed on ice and loaded onto a Superose 12 10/300 gel filtration column equilibrated in buffer GF (20 mM HEPES, pH 7.4, 50 mM NaCl, 1 mM EDTA, 0.002% LMNG) to remove excess detergent and remaining protein contaminants. The purest and the most concentrated fractions of NNT eluted at ~10.5 mL and were concentrated to 5 mg/mL using a Millipore 100-kDa cut-off filter and used immediately for cryo-EM grid preparation (Extended Data Fig. 2). In some purifications, 0.002% LMNG in GF buffer was substituted by 0.05% FOM, which gave a monodisperse and highly active NNT but grids suitable for cryo-EM data collection could not be prepared from FOM preparations as the protein started to aggregate on the grid at concentrations higher than 2 mg/mL. Apo form of our preparation lacked any bound nucleotide, as confirmed by the absence of cyclic reaction without the addition of exogenous $NADP^+$ (data not shown).

Electron microscopy

0.05% CHAPS was added to the protein sample before grid preparation to improve the ice quality and the particle distribution. Substrates at 5 mM concentration were added to the protein 15-30 min before the grid preparation and the samples were incubated on ice. 2.7 μL protein sample was applied to a freshly glow-discharged Quantifoil 0.6/1 copper grid and blotted for 4-6 s using a blotting force of 25 at 4°C and 100% humidity in an FEI Vitrobot Mark IV. Grids were flash-frozen in liquid ethane and stored in liquid nitrogen until data-collection. NNT-$NADP^+$ grids were

imaged using a 300 kV Titan Krios electron microscope equipped with a Gatan energy filtered K2 summit camera with a slit width of 20 eV at The Astbury Centre for Structural Molecular Biology of the University of Leeds. NNT-NADPH grids were imaged using a 300 kV Titan Krios electron microscope equipped with a Gatan energy filtered K2 summit camera with a slit width of 20 eV at the CM01 beamline, ESRF, Grenoble. Images were collected with EPU in a K2 super-resolution mode with a nominal magnification of 130000x and a physical pixel size of 1.065 Å for NNT-$NADP^+$ and 1.07 Å for NNT-NADPH dataset. Total dose of 72 e/$Å^2$ (NNT-$NADP^+$) or 70 e/$Å^2$ (NNT-NADPH) was fractionated into 40 frames of 250 ms each. Apo-NNT grids were imaged using a 300 kV Titan Krios electron microscope equipped with a Gatan energy filtered K3 camera with a slit width of 20 eV at the Institute of Science and Technology Austria. Physical pixel size was 0.84 Å and the total dose of 90 e/$Å^2$ was fractionated into 88 frames of 36 ms each.

Image processing

We collected 2272 movies for the $NADP^+$ dataset, 1722 movies for NADPH dataset and 786 movies for the apo-NNT dataset. The processing was done in RELION 2.1[33] unless otherwise stated. Movie frames were aligned using MotionCor2[34] and initial CTF parameters were estimated from averaged images using CTFFIND[35]. Autopicking with 2D class averages as references resulted in 516395 particles for the NADPH dataset, 1076677 particles for the $NADP^+$ dataset and 500001 particles for the apo dataset. Multiple rounds of 2D classification and 3D classification were performed to classify considerably heterogeneous particles in both datasets (Extended data Fig. 3,4). CTF parameters and per-particle trajectories in the best two classes

451 from the $NADP^+$ dataset were estimated and corrected (particle polishing) using
452 RELION 3.0[36]. Local resolution was estimated using Resmap 5.0[37].
453
454 For the $NADP^+$ dataset we performed one round of 2D classification followed by two
455 rounds of 3D classification with 3x and 2x binned particles, respectively, which
456 resulted in eight classes containing 342284 particles from which it was obvious that
457 there is a considerable heterogeneity in the conformations of dI_2 and dIIIb. To address
458 this, the particles were re-extracted without binning and refined with a dII_2dIII_2 mask
459 to 3.5 Å and then classified into ten classes without searches and without a mask to
460 separate the particles based on the relative position of the dI_2. By combining similar
461 classes and auto-refining them, we separated six different states of NNT which differ
462 from each other with respect to the positions of dI_2 and dIIIb. Two of these classes
463 were resolved to 13 Å, further two to 7 Å and the best two classes to 3.7 and 3.2 Å.
464 From the latter two maps it was obvious that the density for dI_2 was still weaker than
465 for the rest of the particle, indicating remaining heterogeneity in the positions of dI_2,
466 hence the final maps for these two classes were produced by combining focus-refined
467 maps of dII_2dIII_2 and dI_2 parts. This gave the final map for class 1 (closed) with 2.9 Å
468 resolution in the dII_2dIII_2 and 3.2 Å resolution in the dI_2 and for class 2 (open) 3.5 Å
469 resolution for the dII_2dIII and 4.1 Å resolution for the dI_2. Due to the poor quality of
470 the map for the open class in some regions of dIIb (CL6,7,8), we hypothesised that
471 there is still remaining conformational heterogeneity present in this class and we
472 performed another round of classification of these particles with a mask around dIIb
473 to sort out any particles with dIIIb attached/semi-attached to dII. This procedure
474 removed 52% particles and we performed an auto-refinement with a dII_2dIII mask of
475 the remaining 28498 particles with dIIIb unambiguously detached. This resulted in a

3.7 Å map with dIIb density much better resolved and clearly different from the density of dIIa (which has dIII attached) and was used for model building.

For the NADPH dataset, we performed one round of 2D classification followed by one round of 3D classification on 510073 3x binned particles with the same parameters as in the $NADP^+$ dataset, which failed to yield any class with visible secondary structural features. We performed extensive classifications of these particles into 4-20 classes with T values between 4 and 12 and different filtering of the reference volumes which all failed to give a single well-defined class with secondary structural features. Nevertheless, we selected 405141 particles from the best 4 classes from a classification with T=8 and k=6 (same as for $NADP^+$ dataset) for further classification attempts. Another round of extensive classifications was performed on this particle stack with the best results obtained from a T=8, k=20 run. Even in this run only ~6 classes had well-defined features corresponding to the domains of NNT. These 6 classes were re-extracted and refined which gave structures at 8.3, 9.2, 13, 16, 16, and 16 Å and revealed a high degree of dI_2 and dIII mobility (Extended Data Fig. 4a). To address this, we tried to refine the 405141 particles together into one consensus structure at 13 Å, followed by focused refinement of either dI_2 or dII_2 but neither of these strategies yielded structures better than 9 Å, probably due to the too large conformational heterogeneity within the consensus refinement. Furthermore, dI_2 and dII_2 are only 80 kDa each and dII_2 is obscured by a micelle which further complicates the alignment of such a heterogeneous dataset. Finally, we performed multi-body refinement in RELION 3.0 starting from the consensus refinement of 405141 particles and using masks for the two bodies: dI_2 and dII_2. This yielded a 9 Å reconstruction of dI_2 and 10 Å reconstruction of dII_2 but more

501 importantly, the principal component analysis showed the striking degree of dI_2
502 mobility in these particles (Fig. 2de). This is not unexpected as upon dIII dissociation,
503 dI_2 remains only loosely tethered to the rest of the particle by a flexible dI-dII linker.
504
505 The apo-NNT dataset was fully processed in RELION 3.0. We manually selected 643
506 good images and extracted 3x binned particles. Only one conformation of NNT could
507 be observed using various 3D classification schemes, hence the 283706 particles
508 corresponding to it were extracted without binning and auto-refined to 4.5 Å. From
509 this structure it was clear that dI_2 exhibits the same heterogeneity as in the $NADP^+$
510 dataset. To improve the resolution in the dII-dIII, we focus-refined around this region
511 and classified the particles without searches into 6 classes. The best class with 67908
512 particles was auto-refined and polished to reach the resolution of 3.7 Å. Further
513 polishing or subclassification of this class did not improve the resolution further.
514 Attempts at focus-refinement of dI_2 did not improve its resolution compared to the
515 polished full structure of the final selected particles in which local resolution in dI_2
516 was ~5 Å. We conclude that dI_2 without bound nucleotide exhibits even more
517 disorder than when NAD^+ is bound, possibly allowing NAD(H) exchange and dI_2
518 binding/release.
519
520 Model building and refinement
521 The initial model was built into the "double face-down" $NADP^+$ class density by
522 starting with the bovine dIII crystal structure with substituted ovine sequence and the
523 dI homology model that was generated using Phyre2 server[38]. dII model and the
524 linkers were built manually in *Coot*[39]. Manually adjusted models were refined using
525 *PHENIX* software[40] using an adapted method for refining cryo-EM structures which

uses two rounds of a single cycle of group ADP refinement followed by three cycles of global minimization. This allows optimization of B-factors so that electron radiation-damaged carboxylate side-chains acquire high B-factors and do not lead to main-chain distortions (Letts et al, 2019, in press). The final model for NNT is of very high quality in terms of geometry and fit to density (Supplementary Table 1).

Densities for several lipid molecules were observed in each of the half-closed cavities formed by helices TM1, TM2 and TM6 (Extended Data Fig. 5g, 6g-h). They were modelled in the structure as phosphatidylcholines based on their density appearance and the fact that only phosphatidylcholine could reactivate lipid-depleted insect NNT[41].

A density corresponding to the adenylate part of NAD^+ was observed in the NAD(H) binding site of the dI (Extended Data Fig. 5j,k). We propose that this density is NAD^+ which remained bound to the enzyme during purification or, more likely, was introduced into the sample as a contaminant from the $NADP^+$ solution. Our $NADP^+$ was only 98% pure and at 2% NAD^+ contamination, NAD^+ concentration would be 100 μM which is in the range of the K_d for the enzyme[23,28]. The latter is supported by the fact that in our structure the conserved R139 is in the same extended conformation as in the *E. coli* dI_2 with bound NAD^+ and differs significantly from the apo or NADH-bound forms[13]. Nevertheless, our structure is a bona fide oxidised ground state conformation of NNT and earlier biochemical work suggests that nucleotide exchange in dI subunit can happen during any stage of the catalytic cycle and does not influence the global conformation of the enzyme[15,16,42,43]. Models for the "single face-down" $NADP^+$ class and the apo NNT were based on the "double face-down" NNT as the starting model. For apo NNT, due to the lack of reliable amino acid side chain

information in the cryo-EM density of dI domain, dI was modelled as a polyalanine model based on the 6QTI dI and fit into the density as a rigid body.

Structure analysis and preparation of figures

Evolutionary conservation scores were projected onto the transhydrogenase structure using ConSurf[44] (Extended Data Fig. 1b). Buried water molecules were modelled using the original Dowser software (Fig. 3, Extended Data Fig. 7)[45]. Proton translocation pore was predicted and analysed using a MOLEonline server[46]. Interdomain contacts and binding energy of nucleotides were analysed using the PISA server[47,48]. Models were evaluated using MolProbity and EMRinger[49,50]. Clustal Omega was used for sequence alignment[51,52]. Models and density maps were visualised for analysis and figure preparation purposes in PyMOL 2.2.3 and UCSF Chimera[53].

Activity measurements and trypsinolysis

Reverse transhydrogenation activity was measured at 30°C spectrophotometrically by following the $APAD^+$ (3-acetylpyridine adenine dinucleotide; NAD^+ analogue; ε = 5.1 mM^{-1} cm^{-1}) reduction at 375 nm using a Shimadzu UV-2600 UV-VIS spectrophotometer. Background absorption at 455 nm was subtracted from absorption at 375 nm. Reaction buffer was similar to the minimal EDTA-containing buffer used before (20 mM Tris-HCl, pH 6.8, 50 mM NaCl, 0.5 mM EDTA, 0.1% CHAPS, 0.25 mg/mL lipids, 100 μM NADPH and 100 μM $APAD^+$)[25]. For lipids we used soybean asolectin or DOPC:CL 4:1 mixture with similar results. Reaction was started with the addition of NNT. Activity depended on the type of detergent used during the final size exclusion chromatography step. Preparations in FOM gave slightly higher activity

573 (~20 U/mg) than in LMNG (~15 U/mg). These values compare favourably to
574 previous measurements[25,54].
575 Trypsinolysis was performed as described previously with a few changes[15]. NNT at
576 0.05 mg/ml in GF buffer with 1 mM HEPES pH 7.4 was incubated with 0.4 mM
577 nucleotides, trypsin (at different mass ratios) and 60 mM BAT buffer (1:1:1 Bis-Tris,
578 acetate, tricine) at pH 5-8. Due to the pH optimum of trypsin being ~8, mass ratio
579 between 1:400 and 1:40 and incubation times between 30 and 60 min were used at
580 different pH values to achieve comparable rates of proteolysis.
581 Proteoliposome reconstitution
582 NNT was reconstituted into proteoliposomes using a detergent dilution procedure as
583 described before[25]. Briefly, NNT purified in FOM or in LMNG was mixed with a
584 500-fold excess of DOPC solubilised in 1% CHAPS. Following a 10 min incubation
585 on ice, the solution was diluted 100-fold and incubated on ice for 3-5 hours before
586 measuring the activities. Reaction was started by substrate additions (NADPH and
587 $APAD^+$ at 100 μM). CCCP (10 μM) was added after 1 min to decouple the proton
588 gradient across proteoliposomes to assess the dependence of the transhydrogenation
589 reaction on the proton motive force. After another 1 min, CHAPS (0.05%) was added
590 to solubilise proteoliposomes and give a total decoupled reverse transhydrogenation
591 activity of both inward and outward facing transhydrogenases.
592

References

31. Smith, A. L. [13] Preparation, properties, and conditions for assay of mitochondria: Slaughterhouse material, small-scale. *Methods Enzymol.* **10**, 81–86 (1967).

32. Letts, J. A., Degliesposti, G., Fiedorczuk, K., Skehel, M. & Sazanov, L. A. Purification of ovine respiratory complex I results in a highly active and stable preparation. *J. Biol. Chem.* **291**, 24657–24675 (2016).

33. Scheres, S. H. W. RELION: Implementation of a Bayesian approach to cryo-EM structure determination. *J. Struct. Biol.* **180**, 519–530 (2012).

34. Zheng, S. Q. *et al.* MotionCor2: anisotropic correction of beam-induced motion for improved cryo-electron microscopy. *Nat. Methods* **14**, 331–332 (2017).

35. Rohou, A. & Grigorieff, N. CTFFIND4: Fast and accurate defocus estimation from electron micrographs. *J. Struct. Biol.* **192**, 216–221 (2015).

36. Zivanov, J. *et al.* New tools for automated high-resolution cryo-EM structure determination in RELION-3. *Elife* **7**, (2018).

37. Kucukelbir, A., Sigworth, F. J. & Tagare, H. D. Quantifying the local resolution of cryo-EM density maps. *Nat. Methods* **11**, 63–65 (2014).

38. Kelley, L. A., Mezulis, S., Yates, C. M., Wass, M. N. & Sternberg, M. J. E. The Phyre2 web portal for protein modeling, prediction and analysis. *Nat. Protoc.* **10**, 845–58 (2015).

39. Emsley, P., Lohkamp, B., Scott, W. G. & Cowtan, K. Features and development of Coot. *Acta Crystallogr. D. Biol. Crystallogr.* **66**, 486–501 (2010).

40. Adams, P. D. *et al. PHENIX* : a comprehensive Python-based system for macromolecular structure solution. *Acta Crystallogr. Sect. D Biol. Crystallogr.*

66, 213–221 (2010).

41. Vandock, K. P., Emerson, D. J., McLendon, K. E. & Rassman, A. A. Phospholipid Dependence of the Reversible, Energy-Linked, Mitochondrial Transhydrogenase in *Manduca sexta*. *J. Membr. Biol.* **242**, 89–94 (2011).

42. Hu, X., Zhang, J. W., Persson, A. & Rydström, J. Characterization of the interaction of NADH with proton pumping E. coli transhydrogenase reconstituted in the absence and in the presence of bacteriorhodopsin. *BBA - Bioenerg.* **1229**, 64–72 (1995).

43. Tong, R. C. W., Glavas, N. A. & Bragg, P. D. Topological analysis of the pyridine nucleotide transhydrogenase of *Escherichia coli* using proteolytic enzymes. *Biochim. Biophys. Acta* **1080**, 19–28 (1991).

44. Landau, M. *et al.* ConSurf 2005: the projection of evolutionary conservation scores of residues on protein structures. *Nucleic Acids Res.* **33**, W299–W302 (2005).

45. Morozenko, A., Leontyev, I. V & Stuchebrukhov, A. A. Dipole Moment and Binding Energy of Water in Proteins from Crystallographic Analysis. *J. Chem. Theory Comput.* **10**, 4618–4623 (2014).

46. Pravda, L. *et al.* MOLEonline: a web-based tool for analyzing channels, tunnels and pores (2018 update). *Nucleic Acids Res.* **46**, W368–W373 (2018).

47. Krissinel, E. & Henrick, K. Inference of macromolecular assemblies from crystalline state. *J. Mol. Biol.* **372**, 774–97 (2007).

48. Krissinel, E. Crystal contacts as nature's docking solutions. *J. Comput. Chem.* **31**, 133–143 (2010).

49. Barad, B. A. *et al.* EMRinger: side chain–directed model and map validation for 3D cryo-electron microscopy. *Nat. Methods* **12**, 943–946 (2015).

50. Chen, V. B. *et al.* MolProbity: all-atom structure validation for macromolecular crystallography. *Acta Crystallogr. D. Biol. Crystallogr.* **66**, 12–21 (2010).

51. Goujon, M. *et al.* A new bioinformatics analysis tools framework at EMBL-EBI. *Nucleic Acids Res.* **38**, W695–W699 (2010).

52. Larkin, M. A. *et al.* Clustal W and Clustal X version 2.0. *Bioinformatics* **23**, 2947–2948 (2007).

53. Pettersen, E. F. *et al.* UCSF Chimera-A visualization system for exploratory research and analysis. *J. Comput. Chem.* **25**, 1605–1612 (2004).

54. Wu, L. N. Y., Alberta, J. A. & Fisher, R. R. [33] Purification and reconstitution of bovine heart mitochondrial transhydrogenase. *Methods Enzymol.* **126**, 353–360 (1986).

Supplementary Information is linked to the online version of the paper at www.nature.com/nature.

Acknowledgments

We thank Dr Rebecca Thompson from The Astbury Centre for Structural Molecular Biology of the University of Leeds, Dr Gregory Effantin from CM01, ESRF, Grenoble and Dr Victor-Valentin Hodirnau from IST Austria for their assistance with collecting $NADP^+$, NADPH and apo datasets, respectively. Data processing was performed at the IST high-performance computing cluster. This project has received funding from the European Union's Horizon 2020 research and innovation programme under the Marie Skłodowska-Curie Grant Agreement No. 665385.

Author Contributions

DK purified transhydrogenase, prepared cryo-EM grids, acquired and processed EM data, built and analysed the atomic models and wrote the initial draft of the manuscript. LAS designed and supervised the project, acquired funding, analysed data and revised the manuscript.

Author Information

Affiliations: DK & LAS: IST Austria, Am Campus 1, 3400 Klosterneuburg, Austria

Corresponding author: LAS, sazanov@ist.ac.at

The authors declare no competing financial interests.

Data availability statement

Structures of "double face-down" and "single face-down" $NADP^+$ states and apo-NNT were deposited in PDB with PDB access numbers 6QTI, 6QUE and 6S59, respectively, with corresponding cryo-EM density maps in EMDB (EMD-4635, EMD-4637 and EMD-10099).

Extended Data Legends

Extended Data Fig. 1. Comparison of model transhydrogenases from different species (*T. thermophilus, R. rubrum, E. coli, O. aries and H. sapiens*)

a, The domain split and organisation of transhydrogenase in the four model species. dII-dIII linker is conserved in all transhydrogenases, while the dI-dII linker and TM1 are limited to NNTs with α-β polypeptide split (e.g. *E. coli*) and single polypeptide NNTs (metazoans, including mammals). TM5 is only present in metazoans. **b**, Residue conservation scores (calculated in Consurf, coloured cyan to magenta from low to high conservation) mapped on the structure of a single monomer of transhydrogenase. The most highly conserved regions are the proton translocation pathway, nucleotide binding sites and dI-dIII, dII-dIII and dI-dI interfaces. **c**, The architecture of mammalian dII. Supernumerary helices TM1 and TM5 are coloured in a darker shade of blue. Residues of the proton transfer pathway are shown in circles. 3_{10}-helix stretch within TM3 is depicted as a triangular helix. **d**, Alignment of conserved residues on TM3, TM9, TM13, TM14 and CL7 and CL8 important for proton translocation and reaction coupling in *T. thermophilus* (Tt), *R. rubrum* (Rr), *E. coli* (Ec), *O. aries* (Oa) and *H. sapiens* (Hs). *T. thermophilus* and a handful of other species with an NGXGG motif on TM9 have the protonatable histidine on TM3 (α_2H42 in *T. thermophilus*) while most other species that share an HSXXG motif on TM9 have the protonatable histidine on TM9 (βH91 in *E. coli* and H664 in *O. aries*).

Extended Data Fig. 2. Purification and biochemical characterisation of ovine transhydrogenase

a, Ovine NNT was purified chromatographically. The last step of purification, size exclusion chromatography, in two different detergents, FOM and LMNG, is shown. SDS-PAGE shows the presence of ~110 kDa polypeptide of NNT. Highest purity fractions around ~10.5 mL were pooled and concentrated for cryo-EM sample preparation. **c**, NNT is highly active and stable when purified in LMNG as shown by

716 undiminished activity over several days when stored at 4°C. Error bars represent
717 standard deviations based on n=3 independent measurements. **d**, Reconstitution of
718 purified NNT into DOPC liposomes shows that the reverse transhydrogenation
719 reaction is tightly coupled to proton transfer as it is stimulated ~10-fold by proton
720 gradient uncoupler CCCP and by solubilisation in CHAPS detergent. Error bars
721 represent standard deviations based on n=3 independent measurements. **e,**
722 Trypsinolysis of NNT at different pH in the presence of substrates. 110 kDa full NNT
723 and previously identified[15] 66 and 43 kDa fragments are labelled with asterisks. As
724 pH decreases from 8 to 6, NADPH-induced proteolysis diminishes relative to that
725 induced by $NADP^+$. At pH 5 trypsin produces different fragments, but stabilisation of
726 the intact NNT by NADPH is evident. Trypsinolysis was performed independently
727 three times with similar results. NNT purification was repeated independently ten
728 times with similar results as shown in panels a-b. For gel source data, see
729 Supplementary Figure 1.

730

731 **Extended Data Fig. 3. Processing of NNT-$NADP^+$ dataset**

732 Thorough classification of particles resulted in six distinct classes with different
733 domain orientations and resolutions. Best-resolution class ("double face-down" NNT)
734 is almost symmetric with both dIIIs bound in the 'face-down' position while the other
735 five have only one dIII bound in the face-down position and the other dIII detached
736 and the dI_2 tilted at different angles. Simultaneous opening of dI_2 and dissociation of
737 dIIIb is probably necessary to permit full dIIIb rotation during the catalytic cycle.
738 Monomers with dIII detached from dII also show weak or no density for dI-dII linker
739 which suggests that it detaches from dIII to allow dI_2 to open.

740

741 **Extended Data Fig. 4. Processing of Apo-NNT and NNT-NADPH datasets**

742 **a,** NNT bound to NADPH exhibited a large degree of conformational flexibility,
743 which prevented a high-resolution (beyond 8 Å) refinement of any class of particles.
744 Classification into 20 classes revealed that only a small proportion (~5%) of particles

have one dIII bound to dII in the face-down orientation (class C). Another ~10% have partially detached dIII (classes A and B). A vast majority, however, have both dIIIs dissociated from the other domains leading to a large degree of freedom of movement of dI_2 and both dIIIs independently of each other (see classes D, E and F). **b,** Apo-NNT exhibited a single conformational class similar to the "double face-down" NNT class in the presence of $NADP^+$.

Extended Data Fig. 5. Examples of protein and ligand cryo-EM density

All examples are from the "double face-down" class in the presence of $NADP^+$, unless otherwise stated. **a**, Density of the transmembrane helices lining the proton channel (TM3 and 13). **b**, Density comparison of the TM2 between the "double face-down" and "single face-down" (dIII-detached monomer) $NADP^+$ classes, as well as apo class, which remains in the same conformation upon dII opening while TM9 changes (Extended Data Fig. 6c). **c**, Beta sheet density of dI. **d**, Beta sheet density of dIII. **e**, α-helical segment of dI. **f**, α-helical segment of dIII. **g**, Two phosphatidyl-cholines bound in the cavity enclosed by TM1, 2 and 6. **h**, dIIIa-$NADP^+$ density. **i**, dIIIb-$NADP^+$ density. **j**, Partial NAD^+ density in dIa. **k**, Partial NAD^+ density in dIb. The density for lipids and putative NAD^+ is discussed in Methods.

Extended Data Fig. 6. Comparison of "double face-down" and "single face-down" NNT-$NADP^+$ conformations and apo-NNT.

a, Local resolution and FSC curves for the "double face-down" NNT-$NADP^+$ structure. **b**, Local resolution and FSC curves for the "single face-down" NNT-$NADP^+$ structure. **c**, Local resolution and FSC curves for the apo NNT structure. **d**, Overall comparison of "double face-down" (cyan) and "single face-down" (green) classes of NNT. An increased dI tilt, dIIIb detachment and dIIb conformation change are visible. **e,** Comparison of the two monomers in the "closed" $NADP^+$ class as viewed from the dimerization interface reveals a tilt of dI_2 and asymmetry in dI-dIIIa/b contacts. **f,** Overall comparison of "double face-down" NNT-$NADP^+$ (cyan)

and apo NNT. dII-dIII are in the same conformation and dI_2 is slightly more tilted in the apo-NNT. **g,** Electrostatic surface potential of the proton entry cavities on the matrix (bottom) and IMS sides (top) as well as that of the membrane-facing side (right). **h,** Hydrophobicity of residues on the surface of dII_2 (coloured white to red from hydrophobic to hydrophilic). Surface-exposed tyrosine and tryptophan residues, which often delineate lipid membrane surface, are highlighted in green and the lipid-binding pocket is circled.

Extended Data Fig. 7. Changes in the proton translocation channel upon dIII detachment and comparison between ovine and *T. thermophilus* dII

a, Comparison of *T. thermophilus* dII (salmon, PDB 5UNI) and "double face-down" (dIII attached) ovine dII (cyan, supernumerary TM1 and TM5 in blue). Residues in the N-side cavity display markedly different conformations. **b**, Comparison of *T. thermophilus* dII (salmon, PDB 5UNI) and "single face-down" (dIII-detached monomer) ovine dII (blue). Residues in the N-side cavity match more closely as both of these dII structures are detached from dIII. **c**, Comparison of the TM9 density in the "double face-down", "single face-down" (dIII-detached monomer) and apo dII clearly displaying a H664 flip in the dIII-detached dII. **d**, Comparison of Dowser-predicted waters in the dIII-attached (cyan) and dIII-detached (green) dII. The dIII-attached structure has two water molecules, one below and one above the N-side proton gate while the dIII-detached structure only has one water molecule above the gate, consistent with the proposal that channel is open to P-side when dIII is attached. **e**, Density for a water molecule coordinated between H664 and S492, consistent with Dowser-predicted water is beginning to show in our cryo-EM density. **f**, Proton pathway profile (calculated in Mole 2.5) in dIII-attached dII reveals a diameter constriction between N-side and H664, a hydrophobic stretch between H664 and E806 and a negatively charged P-side proton entry site. **g**, Proton pathway profile in the dIII-detached dII. Additional constriction appearing between H664 and P-side upon dIII detachment is indicated.

Extended Data Fig. 8. Different conformations of dIII

a, A homology model of the asymmetric ovine NNT based on the *T. thermophilus* dI_2dIII heterotrimer structure (PDB 4J16). N.B. putative interacting residues at the dIIIup-dIIIdown interface. dI-dII linker contacts the loop D of dIII in the face-down conformation. D942 and Y941 from dIII form hydrogen bonds with R544 on CL2 loop stabilising the dII-dIII interface. Helix 4 and loop D also contribute towards formation of the dI-dIII interface but Y941 is too far to interact with dI. **b,** Comparison of ovine dIII (red) with *R. rubrum* isolated dIII (PDB 1PNO: chain A in blue and chain B in green). Helix 4, loop D and loop E are all more open around the nucleotide in the ovine structure but the nucleotide is occluded by the interactions from the dII residues (not shown) in the ovine "face-down" structure. **c**, Comparison of the NADP(H) binding site in "double face-down"-NNT (left) and apo-NNT (right). Loop E, K999 and R1000 are disordered in apo-NNT and R925 flips into an outward-facing orientation, opening the site to the solvent.

Extended Data Fig. 9. Validation of the mechanism and the reverse transhydrogenation mechanism

a, Summary of the biochemical evidence and mutagenesis data supporting the proposed mechanism. Full description of mutants in *E. coli*, *R. rubrum* and human patient mutations are in Supplementary Tables 1-3. **b**, Our proposal for reverse reaction. Reverse transhydrogenation reaction consumes NADPH and NAD^+ and results in proton pumping, supporting proton motive force (pmf). The driving forces for this reaction are the nucleotide ratios and low pmf which promotes protonation of H664 from the matrix side.

Extended Data Table 1. Cryo-EM data collection, refinement and validation statistics

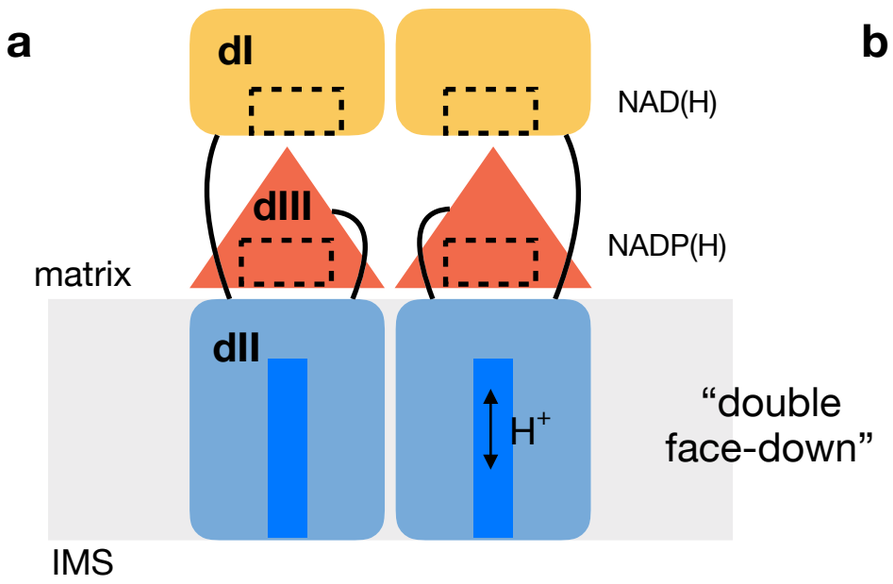
a
dI
dIII
dII
NAD(H)
NADP(H)
matrix
IMS
H+
“double face-down”
~100 Å
~130 Å
90°

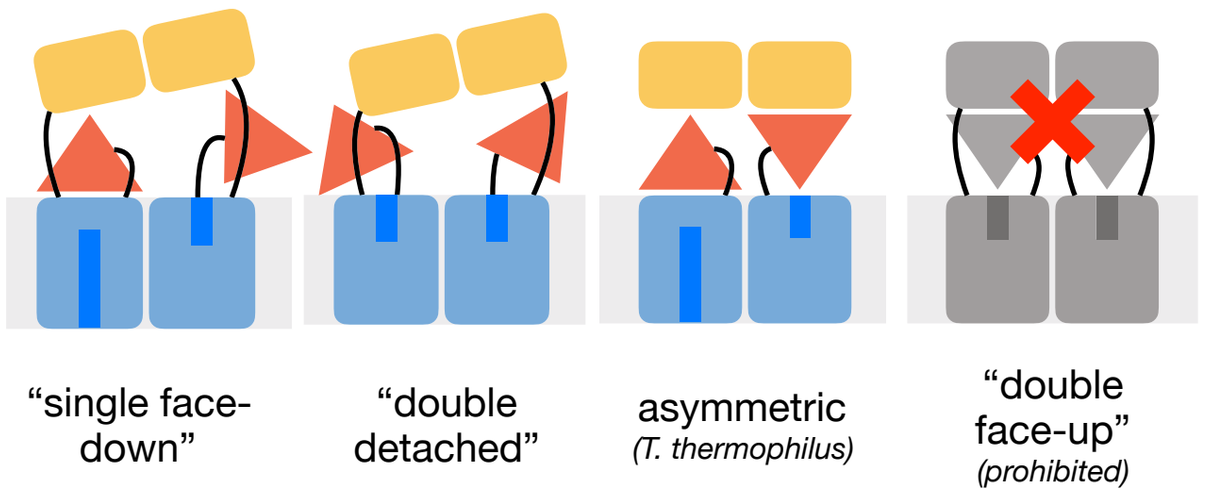
b
“single face-down”
“double detached”
asymmetric
(T. thermophilus)
“double face-up”
(prohibited)

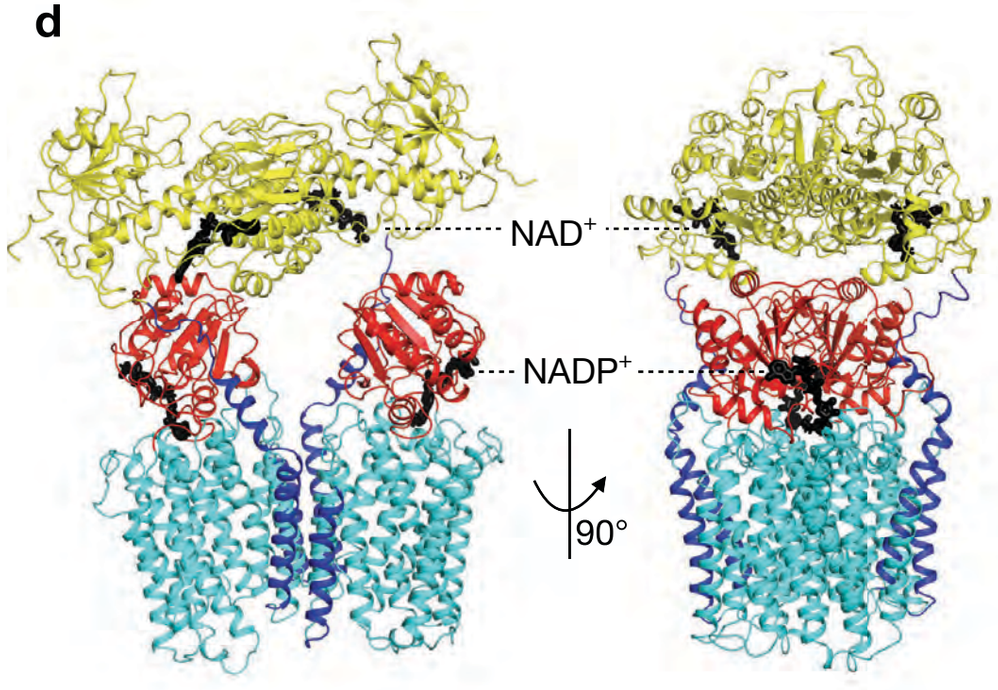
d
NAD+
NADP+
90°

Fig. 1

a

Apo: “double face-down”

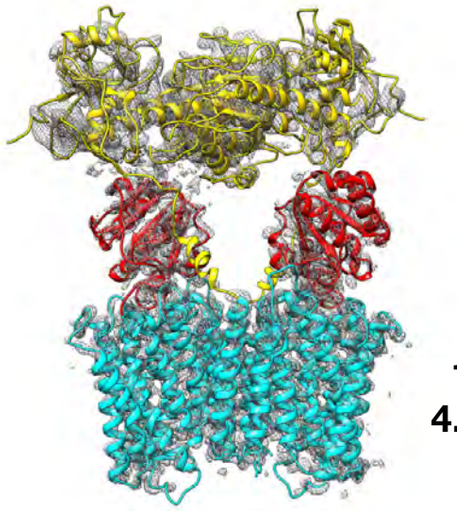

100 %
4.2/3.7 Å

NADP$^+$: “double face-down”

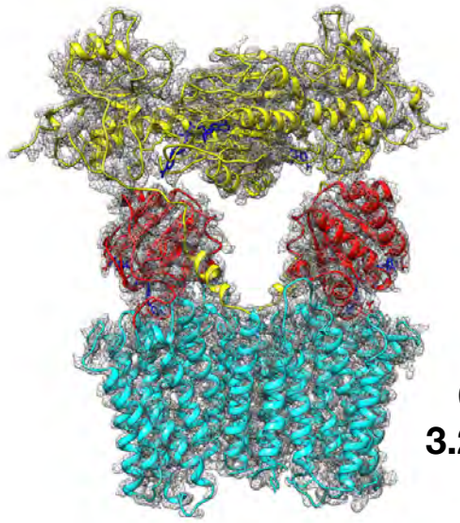

63 %
3.2/2.9 Å

NADP$^+$: “single face-down”

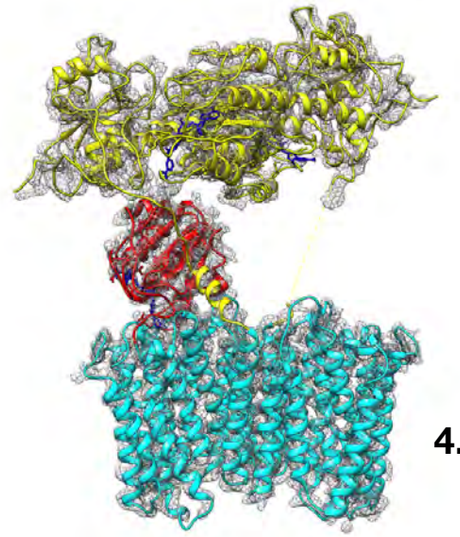

18 %
4.1/3.7 Å

NADPH: “single face-down”

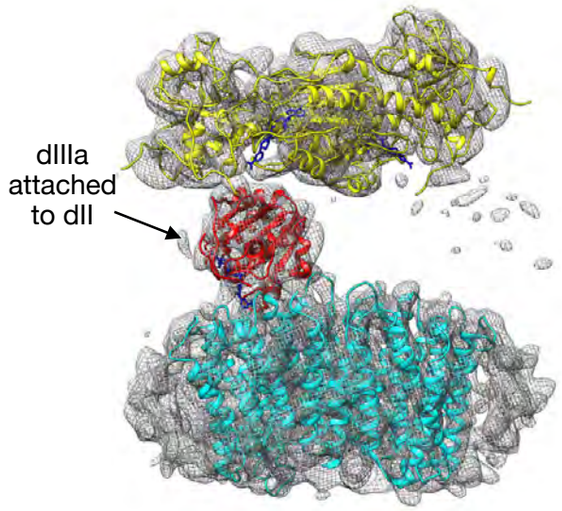

11 %
8.6 Å

NADPH: “double detached”

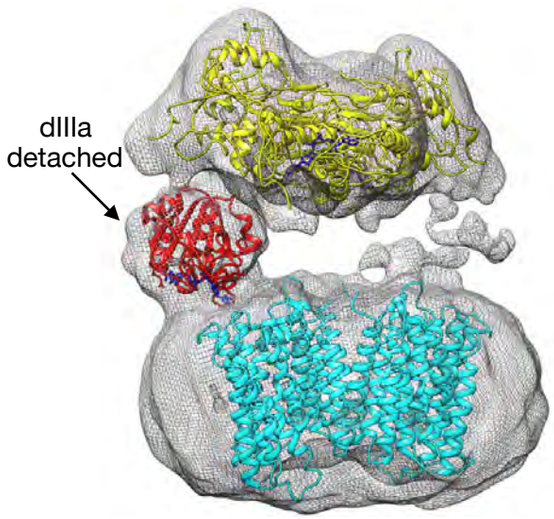

11 %
9.2 Å

NADPH: “double detached”

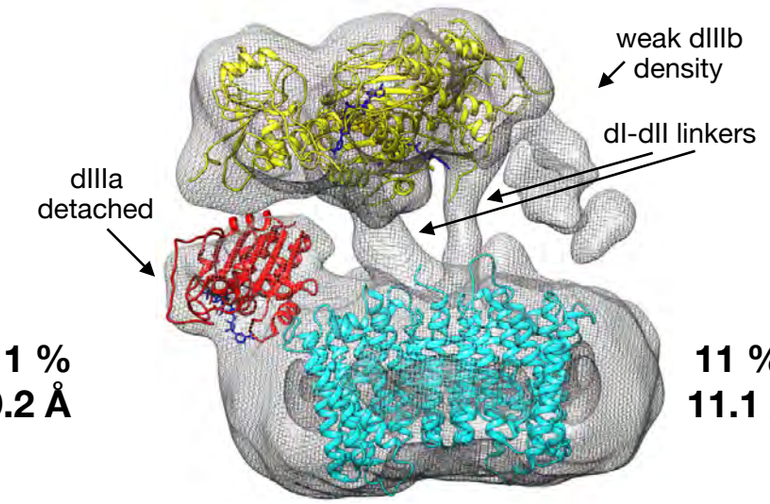

11 %
11.1 Å

b

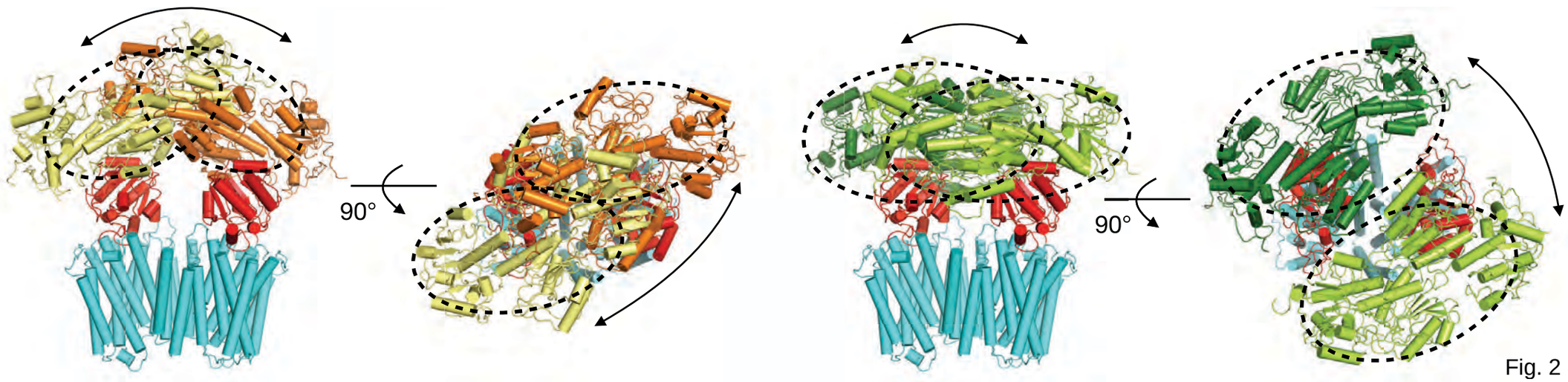

Fig. 2

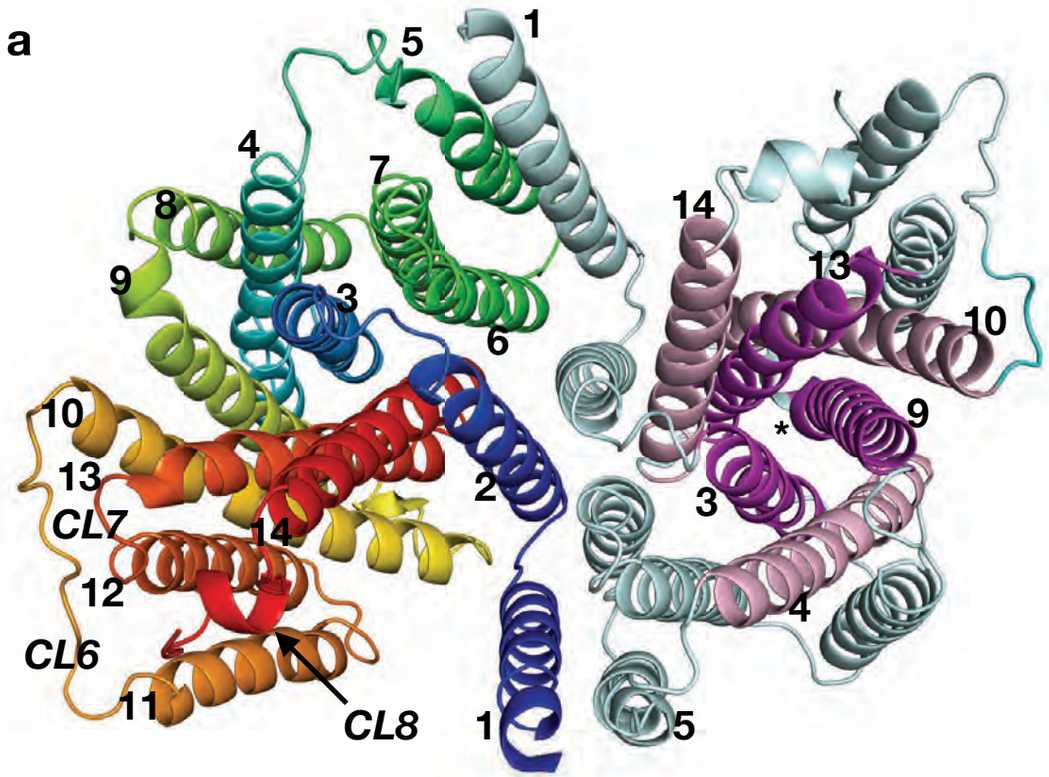
a
1
5
4
7
8
9
3
6
10
13
CL7
14
12
CL6
11
CL8
2
1
14
13
10
9
*
3
4
5

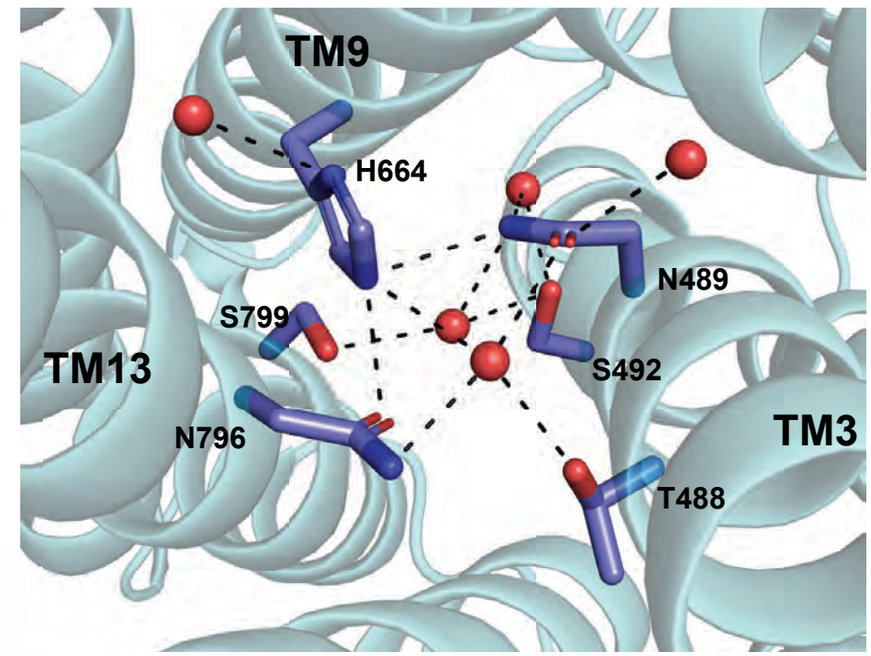
d
TM9
H664
N489
S799
TM13
S492
N796
TM3
T488

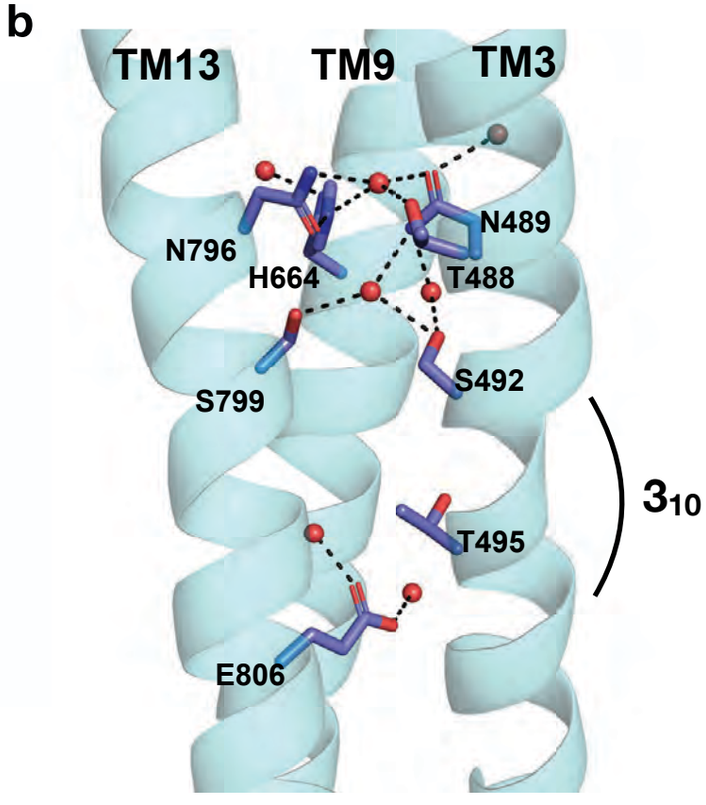
b
TM13
TM9
TM3
N796
H664
N489
T488
S799
S492
T495
E806
3₁₀

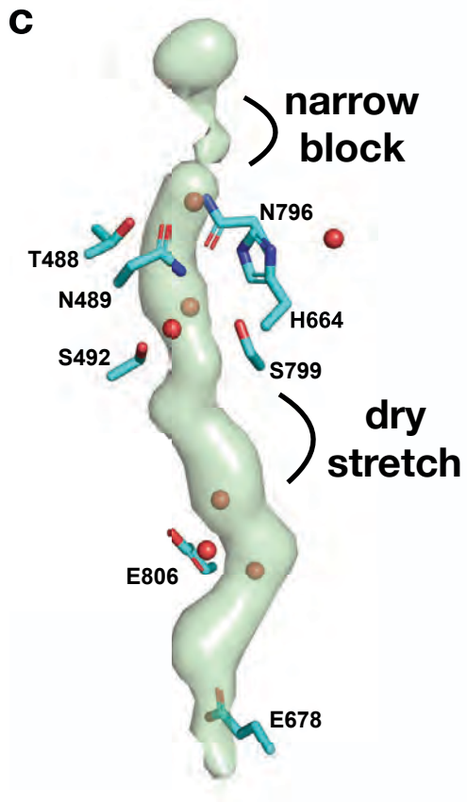
c
narrow block
N796
T488
N489
H664
S492
S799
dry stretch
E806
E678

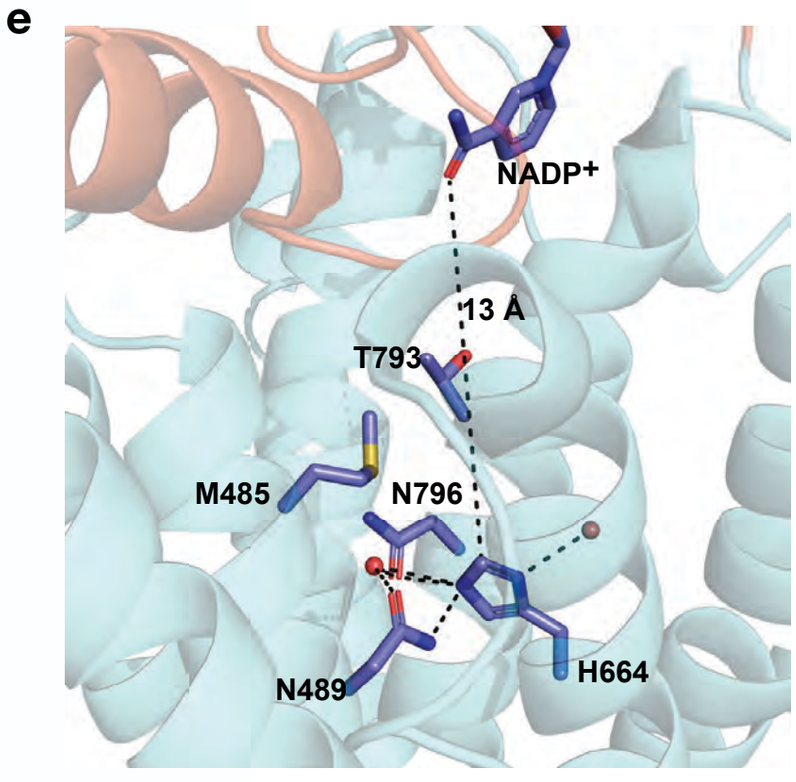
e
NADP+
13 Å
T793
M485
N796
N489
H664

Fig. 3

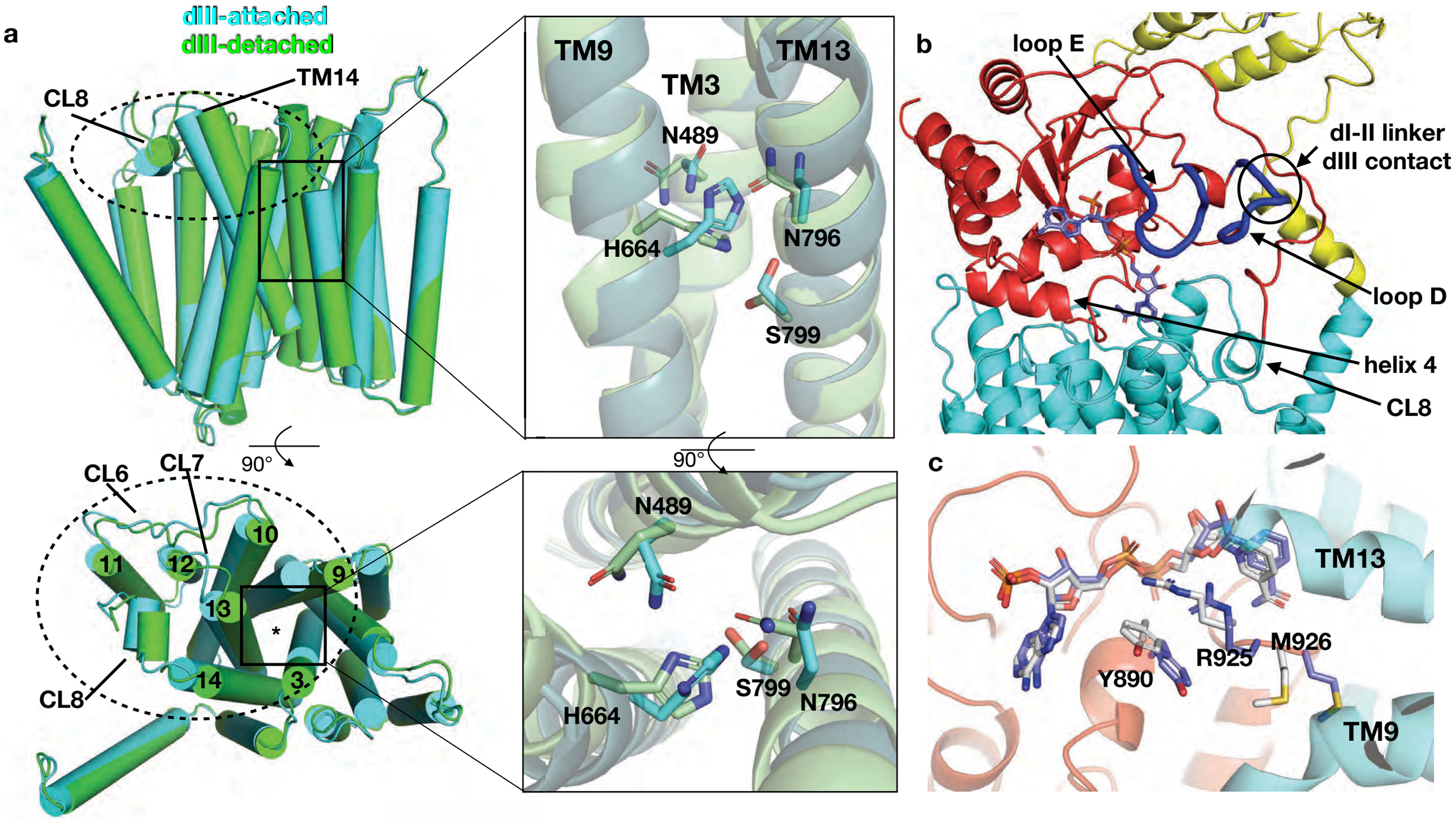
a
dIII-attached
dIII-detached
TM14
CL8
CL6
CL7
90°
10
11
12
9
13
*
14
3
CL8
TM9
TM13
TM3
N489
H664
N796
S799
90°
N489
S799
N796
H664
b
loop E
dI-II linker
dIII contact
loop D
helix 4
CL8
c
TM13
M926
R925
Y890
TM9

Fig. 4

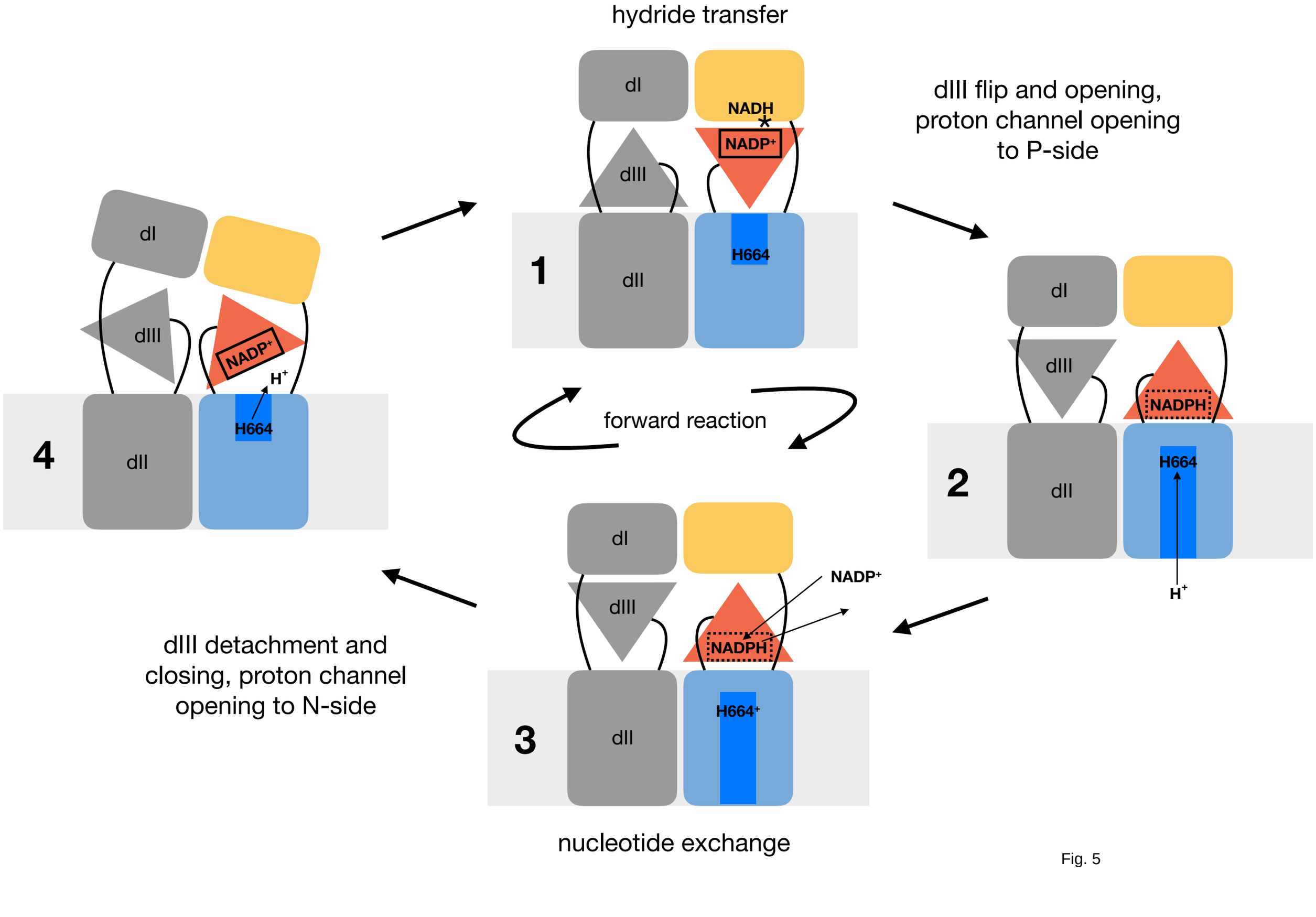
hydride transfer
dI
NADH
*
NADP+
dIII
1
dII
H664
dIII flip and opening,
proton channel opening
to P-side
dI
dIII
NADPH
H664
2
dII
H+
NADP+
dIII detachment and
closing, proton channel
opening to N-side
dI
dIII
NADPH
3
dII
H664+
nucleotide exchange
dI
NADP+
H+
4
dII
H664
forward reaction

Fig. 5

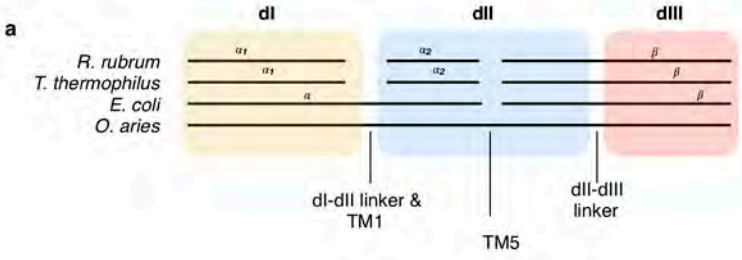
a
dI
dII
dIII
R. rubrum
T. thermophilus
E. coli
O. aries
dI-dII linker & TM1
TM5
dII-dIII linker

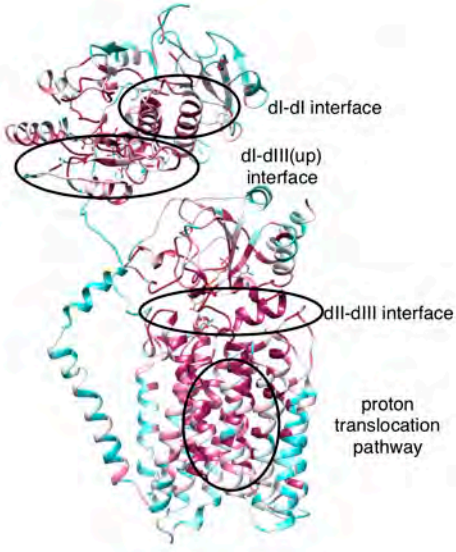
b
dI-dI interface
dI-dIII(up) interface
dII-dIII interface
proton translocation pathway

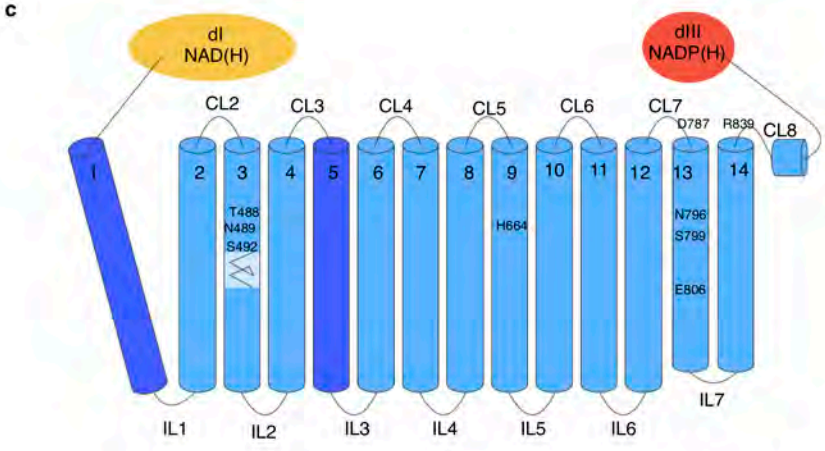
c
dI NAD(H)
dIII NADP(H)
CL2
CL3
CL4
CL5
CL6
CL7
CL8
D787
R839
T488
N489
S492
H664
N796
S799
E806
IL1
IL2
IL3
IL4
IL5
IL6
IL7

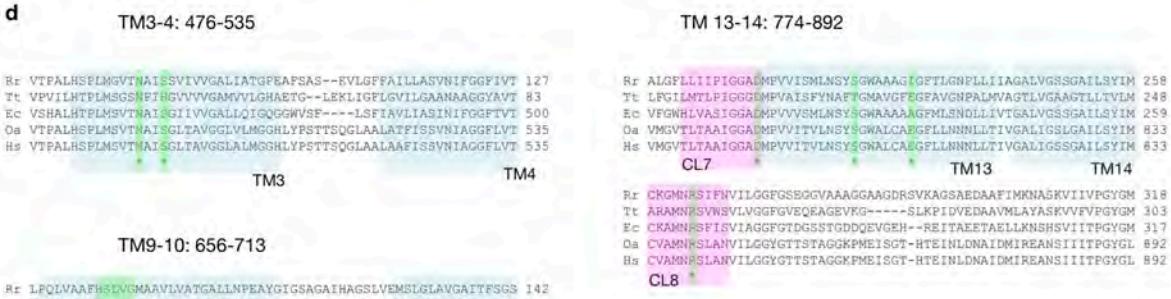
d
TM3-4: 476-535
TM3
TM4
TM 13-14: 774-892
CL7
TM13
TM14
TM9-10: 656-713
TM9
TM10
CL8

ED 1

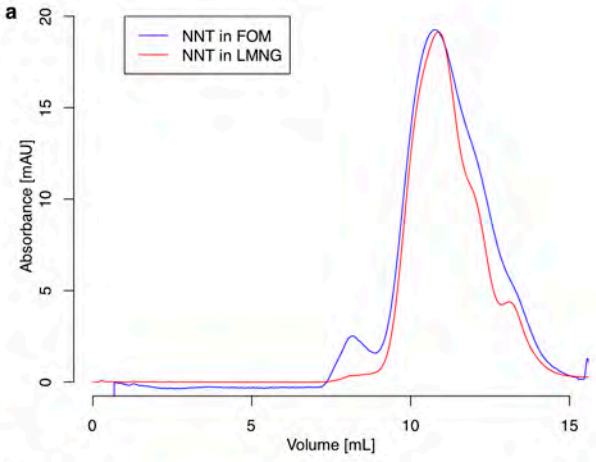
a
NNT in FOM
NNT in LMNG
Absorbance [mAU]
Volume [mL]

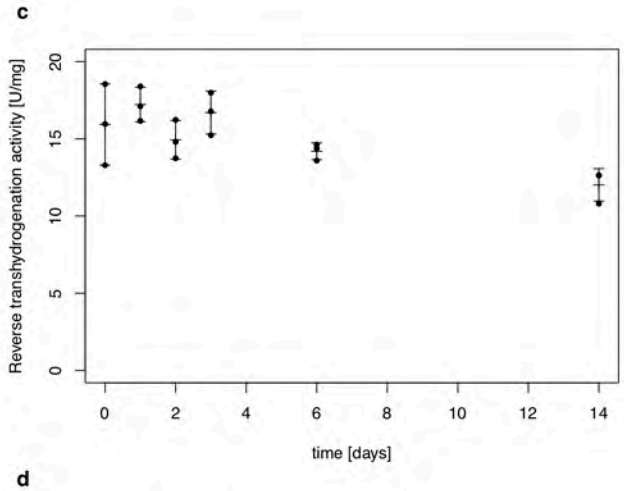
c
Reverse transhydrogenation activity [U/mg]
time [days]

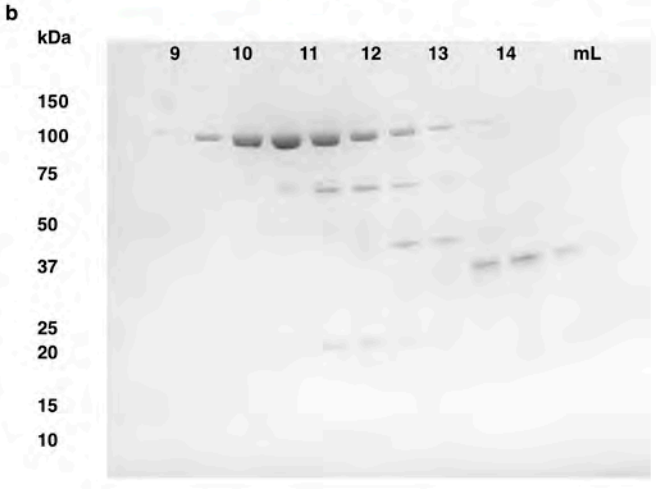
b
kDa
9
10
11
12
13
14
mL

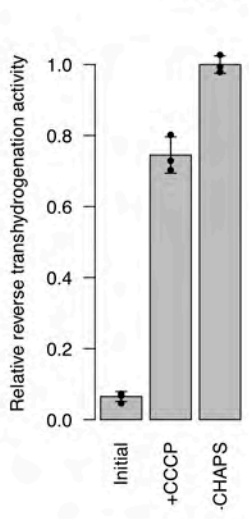
d
Relative reverse transhydrogenation activity
Initial
+CCCP
-CHAPS

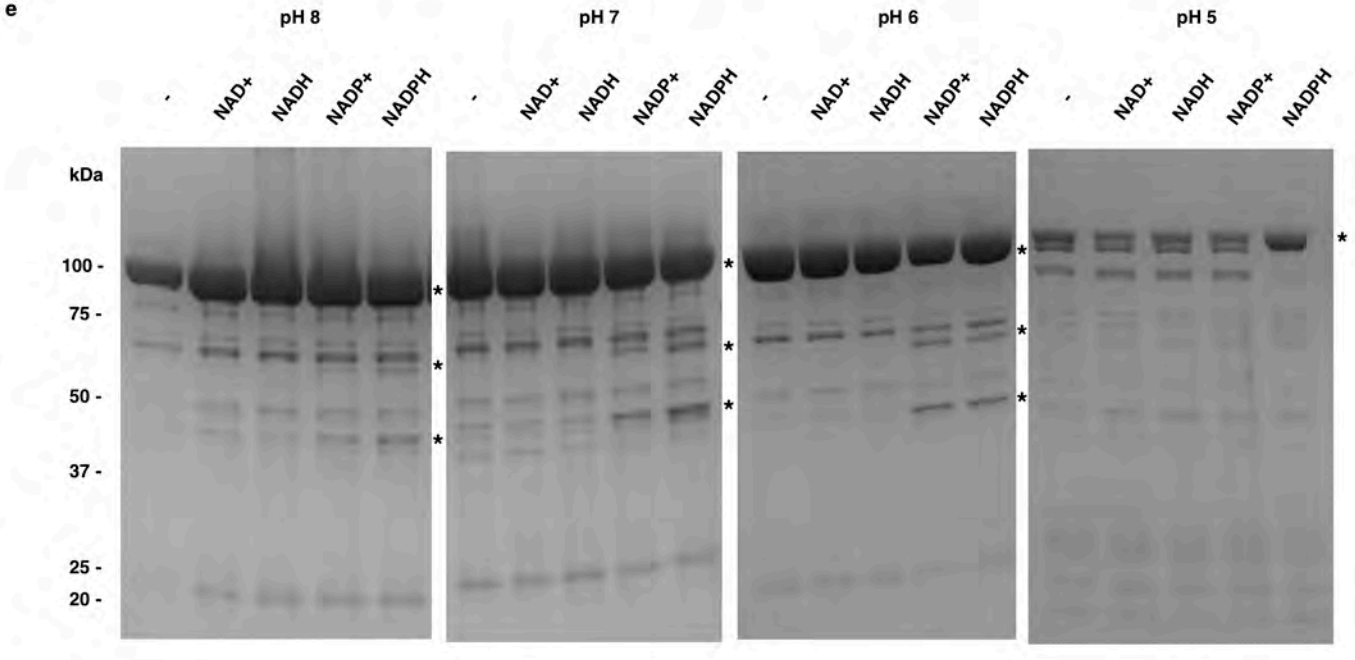
e
pH 8
pH 7
pH 6
pH 5
-
NAD+
NADH
NADP+
NADPH
kDa

ED 2

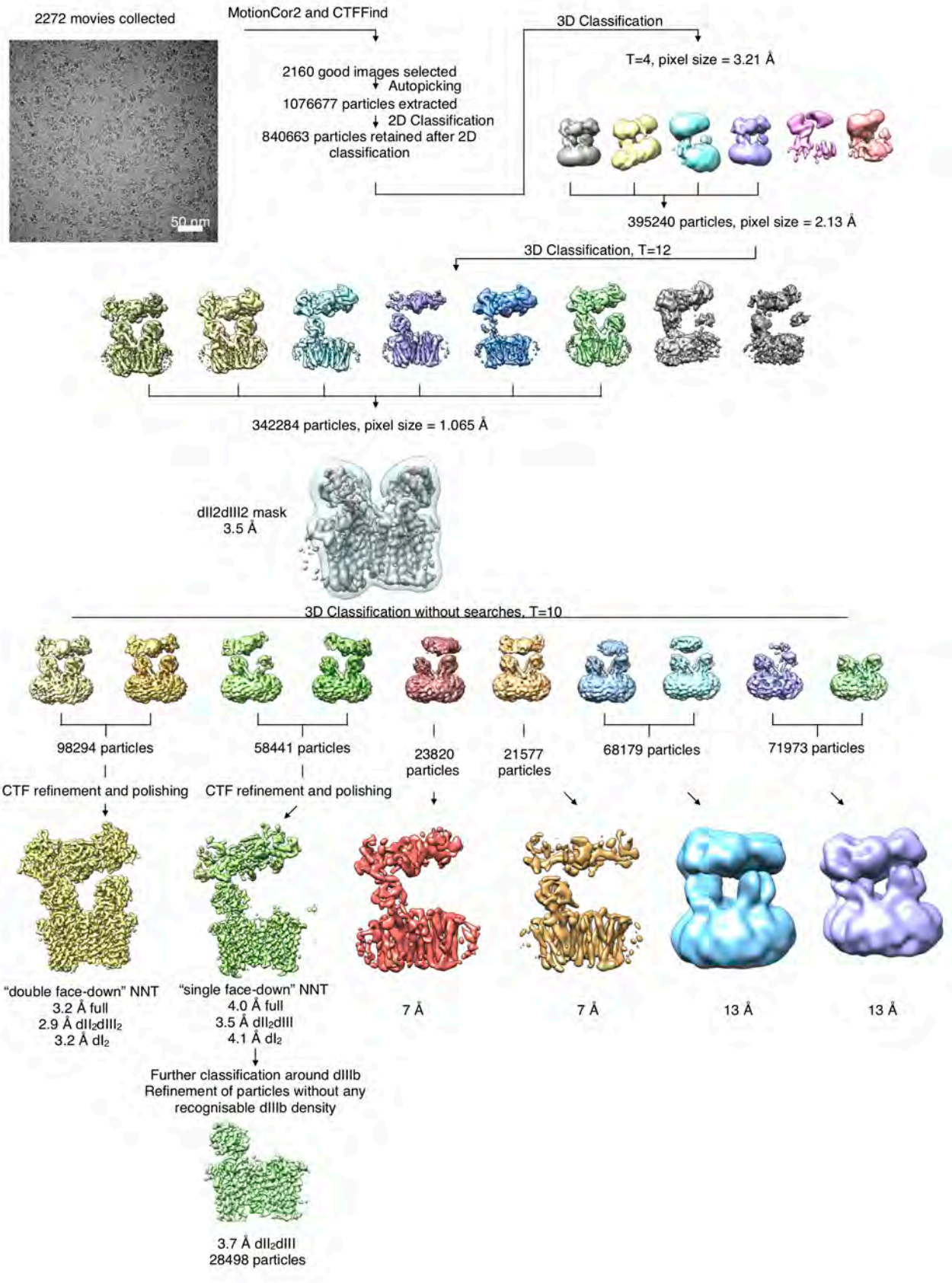
2272 movies collected
50 nm
MotionCor2 and CTFFind
2160 good images selected
Autopicking
1076677 particles extracted
2D Classification
840663 particles retained after 2D classification
3D Classification
T=4, pixel size = 3.21 Å
395240 particles, pixel size = 2.13 Å
3D Classification, T=12
342284 particles, pixel size = 1.065 Å
dII2dIII2 mask
3.5 Å
3D Classification without searches, T=10
98294 particles
58441 particles
23820 particles
21577 particles
68179 particles
71973 particles
CTF refinement and polishing
CTF refinement and polishing
"double face-down" NNT
3.2 Å full
2.9 Å dII2dIII2
3.2 Å dI2
"single face-down" NNT
4.0 Å full
3.5 Å dII2dIII
4.1 Å dI2
7 Å
7 Å
13 Å
13 Å
Further classification around dIIIb
Refinement of particles without any recognisable dIIIb density
3.7 Å dII2dIII
28498 particles

ED 3

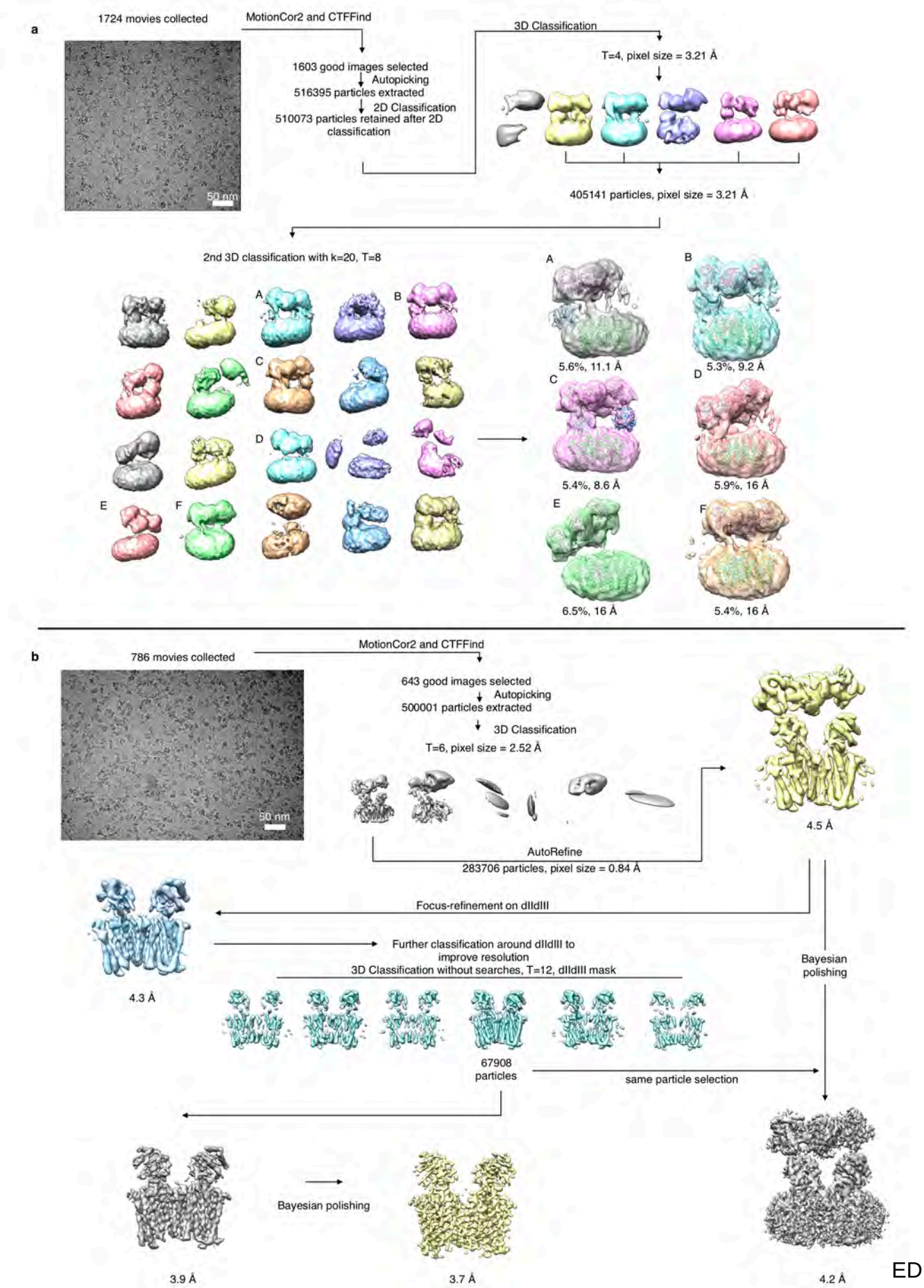
a
1724 movies collected
50 nm
MotionCor2 and CTFFind
1603 good images selected
Autopicking
516395 particles extracted
2D Classification
510073 particles retained after 2D classification
3D Classification
T=4, pixel size = 3.21 Å
405141 particles, pixel size = 3.21 Å
2nd 3D classification with k=20, T=8
A
B
C
D
E
F
5.6%, 11.1 Å
5.3%, 9.2 Å
5.4%, 8.6 Å
5.9%, 16 Å
6.5%, 16 Å
5.4%, 16 Å
b
786 movies collected
50 nm
MotionCor2 and CTFFind
643 good images selected
Autopicking
500001 particles extracted
3D Classification
T=6, pixel size = 2.52 Å
AutoRefine
283706 particles, pixel size = 0.84 Å
4.5 Å
Focus-refinement on dIIdIII
4.3 Å
Further classification around dIIdIII to improve resolution
3D Classification without searches, T=12, dIIdIII mask
Bayesian polishing
67908 particles
same particle selection
Bayesian polishing
3.9 Å
3.7 Å
4.2 Å

ED 4

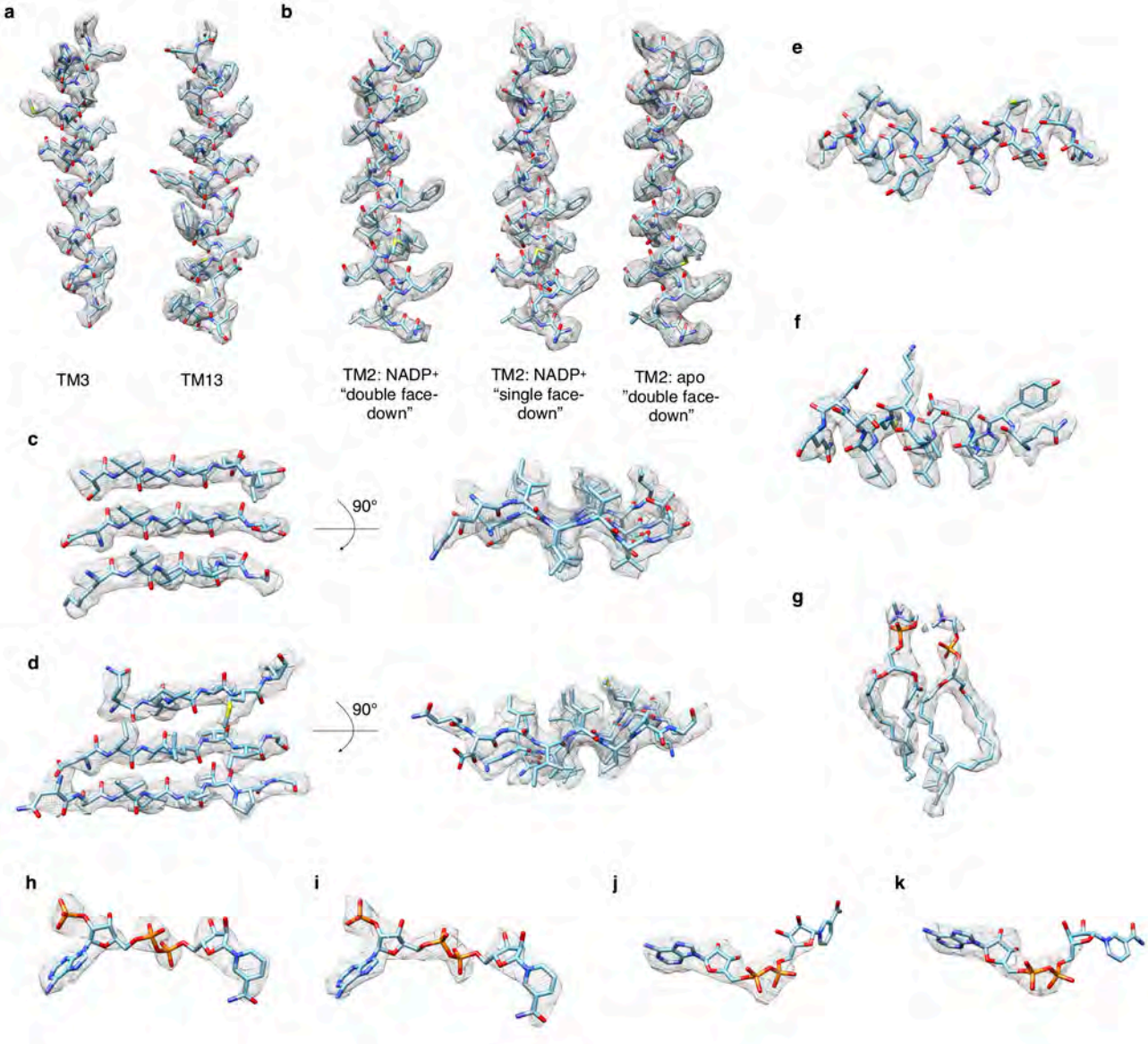
a
b
e
TM3
TM13
TM2: NADP+ "double face-down"
TM2: NADP+ "single face-down"
TM2: apo "double face-down"
f
c
90°
d
90°
g
h
i
j
k

ED 5

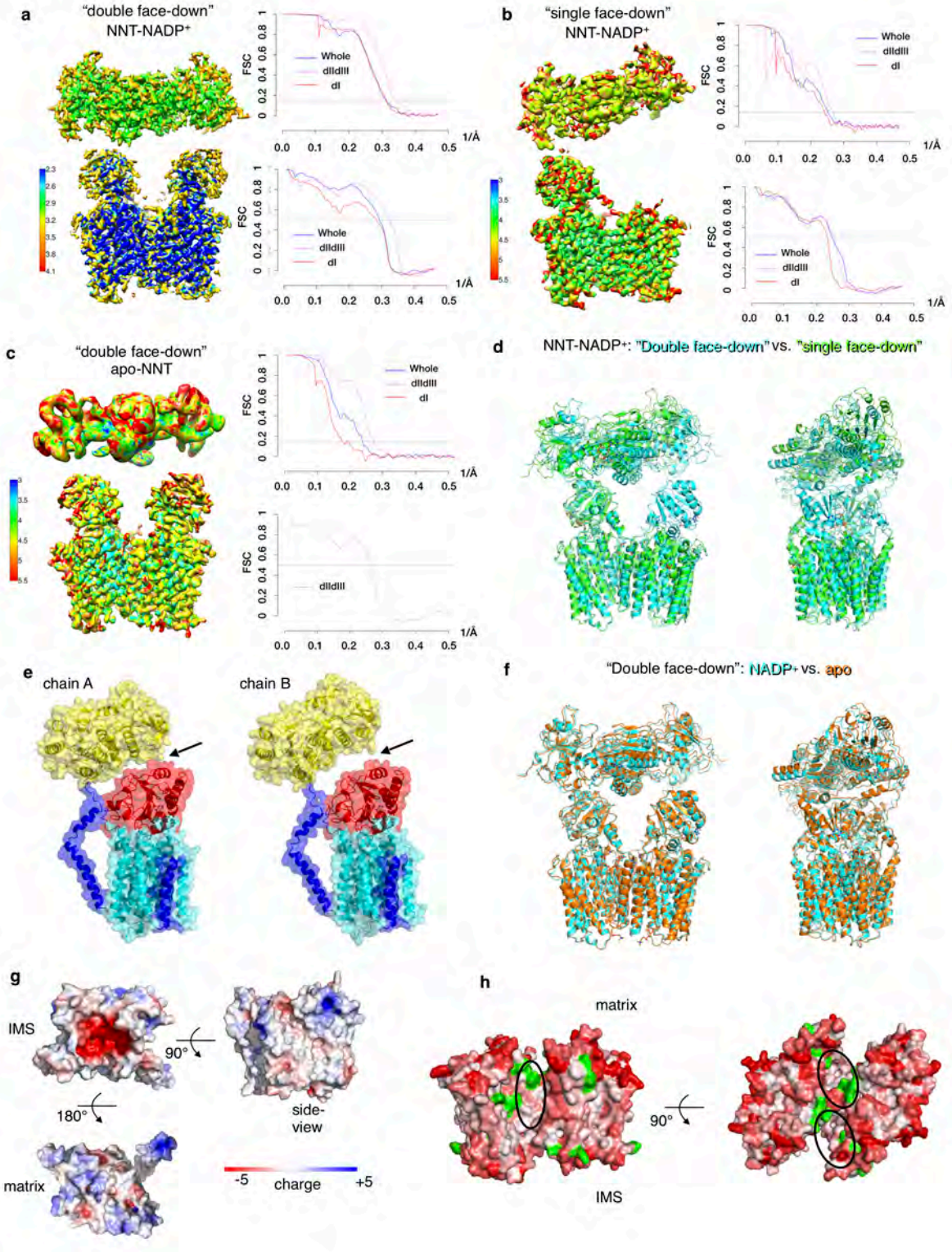
a
"double face-down"
NNT-NADP+
FSC
Whole
dIIdIII
dI
1/Å
b
"single face-down"
NNT-NADP+
c
"double face-down"
apo-NNT
d
NNT-NADP+: "Double face-down" vs. "single face-down"
e
chain A
chain B
f
"Double face-down": NADP+ vs. apo
g
IMS
90°
180°
side-
view
matrix
-5
charge
+5
h
matrix
90°
IMS

ED 6

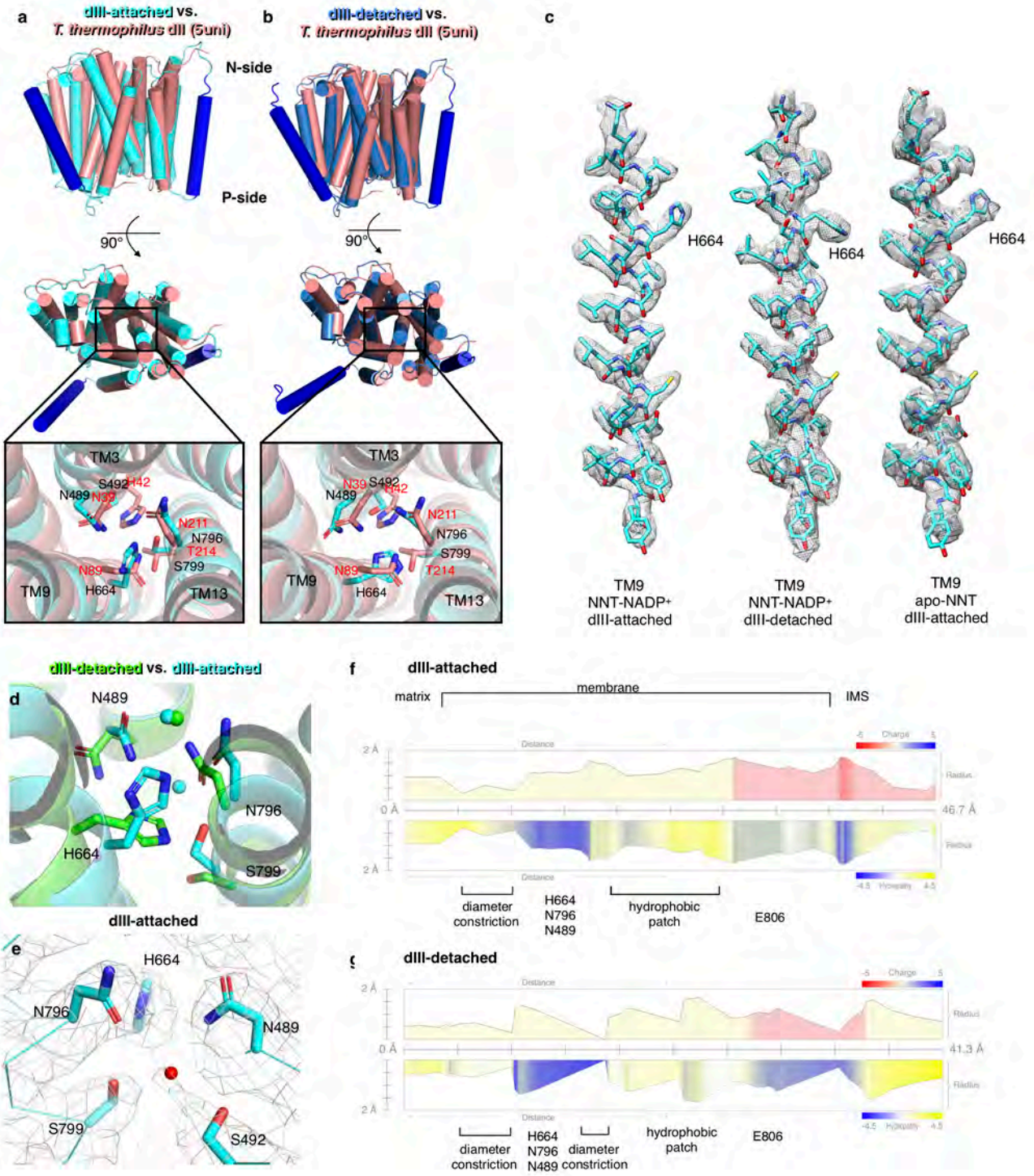
a
dIII-attached vs.
T. thermophilus dII (5uni)
b
dIII-detached vs.
T. thermophilus dII (5uni)
N-side
P-side
90°
90°
TM3
S492
H42
N489
N39
N211
N796
T214
S799
N89
TM9
H664
TM13
c
H664
H664
H664
TM9
NNT-NADP+
dIII-attached
TM9
NNT-NADP+
dIII-detached
TM9
apo-NNT
dIII-attached
dIII-detached vs. dIII-attached
d
N489
N796
H664
S799
dIII-attached
e
H664
N796
N489
S799
S492
f
dIII-attached
matrix
membrane
IMS
Distance
Charge
Radius
Hydropathy
46.7 Å
diameter
constriction
H664
N796
N489
hydrophobic
patch
E806
g
dIII-detached
41.3 Å
diameter
constriction
H664
N796
N489
diameter
constriction
hydrophobic
patch
E806

ED 7

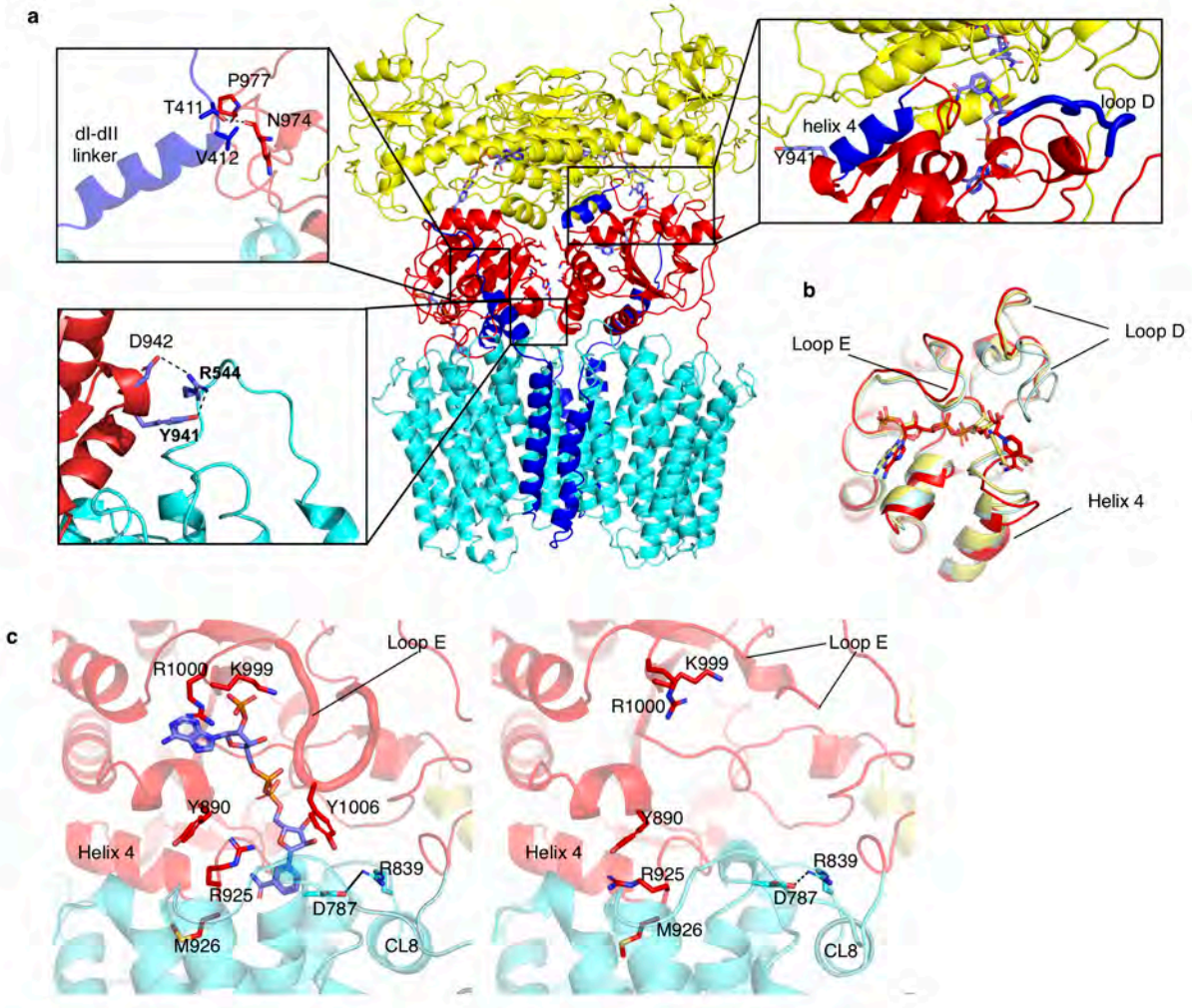
a
P977
T411
N974
dI-dII
linker
V412
D942
R544
Y941
helix 4
Y941
loop D
b
Loop E
Loop D
Helix 4
c
R1000
K999
Loop E
Y890
Y1006
Helix 4
R925
R839
D787
M926
CL8
K999
Loop E
R1000
Y890
Helix 4
R925
R839
D787
M926
CL8

ED 8

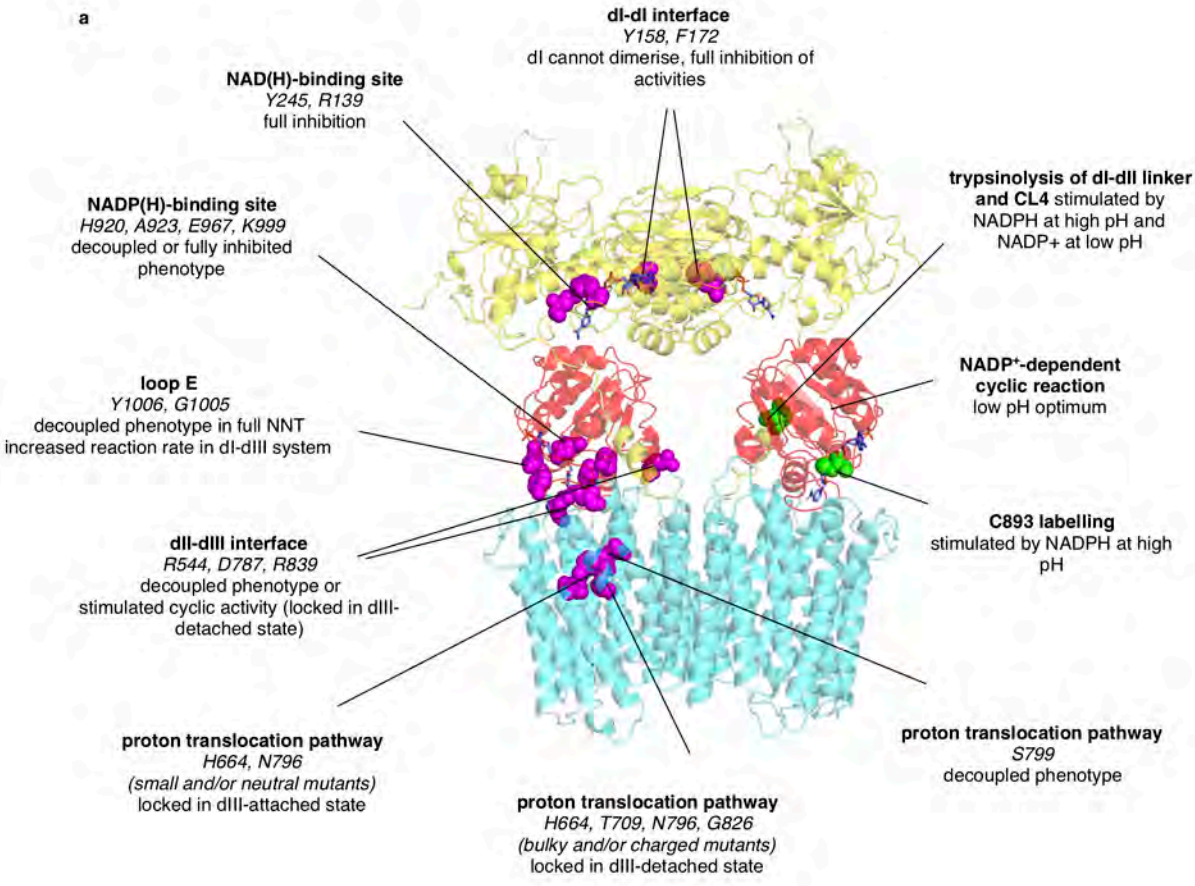
a
dI-dI interface
Y158, F172
dI cannot dimerise, full inhibition of activities
NAD(H)-binding site
Y245, R139
full inhibition
NADP(H)-binding site
H920, A923, E967, K999
decoupled or fully inhibited phenotype
trypsinolysis of dI-dII linker and CL4 stimulated by NADPH at high pH and NADP+ at low pH
loop E
Y1006, G1005
decoupled phenotype in full NNT
increased reaction rate in dI-dIII system
NADP+-dependent cyclic reaction
low pH optimum
C893 labelling
stimulated by NADPH at high pH
dII-dIII interface
R544, D787, R839
decoupled phenotype or stimulated cyclic activity (locked in dIII-detached state)
proton translocation pathway
H664, N796
(small and/or neutral mutants)
locked in dIII-attached state
proton translocation pathway
S799
decoupled phenotype
proton translocation pathway
H664, T709, N796, G826
(bulky and/or charged mutants)
locked in dIII-detached state

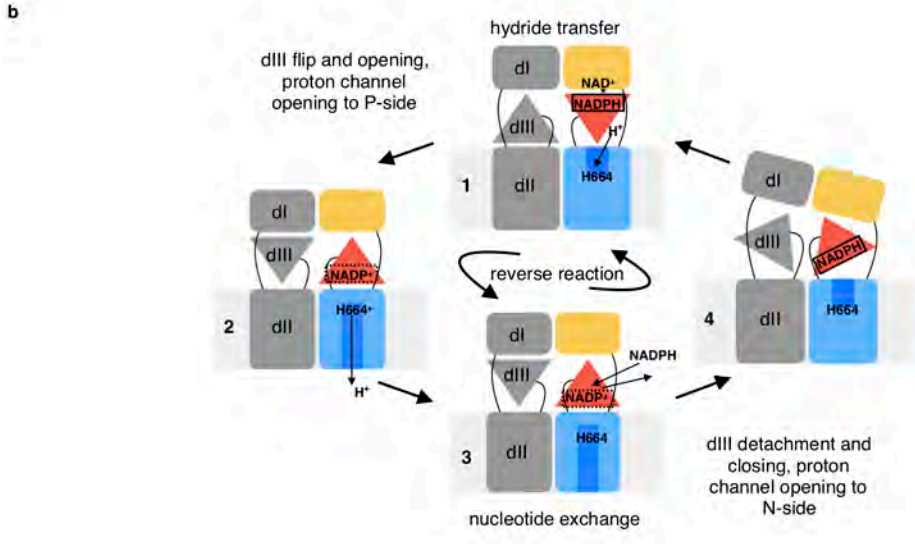
b
hydride transfer
dIII flip and opening, proton channel opening to P-side
dI
dII
dIII
NAD+
NADPH
H+
H664
1
2
3
4
NADP+
H664+
reverse reaction
dIII detachment and closing, proton channel opening to N-side
nucleotide exchange

	NNT-NADP+ "double face-down" (EMD-4635) (PDB 6QTI)	NNT-NADP+ "single face-down" (EMD-4637) (PDB 6QUE)	Apo-NNT "double face-down" (EMDB-10099) (PDB 6S59)
Data collection and processing			
Magnification	130000x	130000x	130000x
Voltage (kV)	300	300	300
Electron exposure (e–/Å^2)	72	72	90
Defocus range (μm)	~ -1 to -2.5	~ -1 to -2.5	~ -1 to -2.5
Pixel size (Å)	1.065	1.065	0.84
Symmetry imposed	C1	C1	C1
Initial particle images (no.)	1076677	1076677	500001
Final particle images (no.)	98294	58441	67908
Map resolution (Å)	dI_2 – 3.2 Å, dII_2dIII_2 – 2.9 Å	dI_2 – 4.2 Å, dII_2dIII – 3.7 Å	dI_2 – 4.5 Å, dII_2dIII_2 – 3.7 Å
FSC threshold	0.143	0.143	0.143
Refinement			
Initial model used (PDB code)	dI and dII built de novo, dIII based on 1D4O	6QTI	6QTI
Model resolution (Å)	dI_2 – 3.4 Å, dII_2dIII_2 – 3.1 Å	dI_2 – 4.3 Å, dII_2dIII – 4.0 Å	dII_2dIII_2 – 3.8 Å
FSC threshold	0.5	0.5	0.5
Map sharpening *B* factor (Å^2)	dII_2dIII_2 -36.2 dI_2 -50.2	dII_2dIII -55 dI_2 -77.0	dII_2dIII_2 -67.3 dI_2 -197.5
Model composition			
Non-hydrogen atoms	15996	13791	13397
Protein residues	2076	1865	2066
Ligands	14	3	8
B factors (Å^2)			
Protein	74.0	128.0	115.8
Ligand	114.8	172.8	143.5
R.m.s. deviations			
Bond lengths (Å)	0.0071	0.008	0.0085
Bond angles (°)	1.29	1.30	1.36
Validation			
MolProbity score	1.56	1.66	1.59
EMRinger score	3.58	1.73	2.53
Clashscore	3.37	4.26	3.50
Poor rotamers (%)	0	0.21	0.44
Ramachandran plot			
Favored (%)	93.44	92.85	92.95
Allowed (%)	6.56	7.05	7.05
Disallowed (%)	0	0.1	0

ED 10

Supplementary Information

Supplementary Discussion

Mammalian-specific features of NNT

The twelve conserved transmembrane helices in mammalian NNT adopt the same fold as demonstrated in the isolated *T. thermophilus* dII domain[1,2]. The supernumerary helices TM1 and TM5 form an unexpected extended dII dimer interface. Relatively large tilt of the TM1 allows its strong association over a large contact area with the TM5 of the opposite monomer, possibly stabilizing dimer formation in mammals (Fig. 3a). The connection from the dI domain via TM1 to TM5 of the opposing monomer may also help in the coordination of the catalytic cycle events between the monomers as discussed below.

The dI-dII linker present in transhydrogenases with single and double polypeptide split (Extended Data Fig. 1a) was resolved here for the first time. The C-terminal part of the linker (residues 410-424) forms a loosely defined α helix which contacts dIII in the 'face-down' orientation. V412 and T411 from the linker interact with residues N974-P977 of the loop D (residues 974-986) on dIII. This explains why K410-T411 bond is protected from trypsinolysis in the apo and $NADP^+$-bound state (Fig. 1c,d, Extended Data Fig. 8a)[3]. The N-terminal region of the dI-dII linker (400-410) is a flexible loop and only displays very weak density. In the dIII-detached state, the density for the C-terminal part of the linker disappears, which could indicate partial unfolding of the helix to accommodate an increased distance between dI and dII.

The only catalytically important conformation that we did not observe in our structures is the face-up dIII conformation since it is likely that the dI-dIII interface formation requires binding of the corresponding nucleotide to dI and, once formed, has a very short life span as the hydride transfer is fast[4–6]. In contrast to the bacterial enzymes, the architecture of mammalian NNT with its dI-dII linker may prevent the observation of a stable face-up dIII conformation, although this remains to be established in future studies. Structures of dI_2dIII heterotrimers from *T. thermophilus* and *R. rubrum* demonstrated that only one copy of dIII can bind to dI_2 at a time due to steric clashes[7–10]. The symmetry of the "double face-down" state, most likely specific to single polypeptide transhydrogenases, is broken due to the tilting of dI_2, which interacts loosely with dIII in one monomer (dIIIa) and not at all in another (dIIIb) (Extended Data Fig. 6e). The overall architecture of the dimer does not allow for tight

interactions between dI and dIII in both monomers, whether dIII is facing "up" or "down". On the other hand, dIII-dII interaction is permitted in both monomers simultaneously.

Comparison of proton translocation machinery between ovine and *T. thermophilus* NNT

All transhydrogenases have a single key protonatable histidine at the N-side of dII, either on TM3 (α_2H42 in *T. thermophilus*) or on TM9 in *E. coli* and mammals (βH91/H664) (Extended Data Fig. 1d and 7a,b). MD simulations of *T. thermophilus* enzyme[2] showed that protonation of this histidine induces a transient opening of the transmembrane proton channel between α_2H42 and βE221 (ovine H664 and E806) accompanied by a flip of βT214. This role could be played by the ovine homologue S799 or by S492, a homologue of *T. thermophilus* α_2H42, or by a non-conserved T495 (Fig. 3b)[2]. The latter two residues sit on a clear and significant distortion of helix TM3, i.e. two turns of 3_{10} helix (the only such distortion in dII, Fig. 3b). A similar distortion is present (but was not discussed) around α_2H42 in the TM3 of *T. thermophilus* dII (PDB 5UNI and 4O93). Furthemore, in TM9, the backbone oxygen atoms of residues 661, 662 and 667 are facing away from the helix-forming hydrogen bond network. Such disruptions of secondary structure in TM helices happen almost exclusively in functionally important sites, where flexibility of otherwise rigid TM helices is required[11,12], consistent with our conclusion that these key TM3 and TM9 residues undergo conformational changes associated with proton translocation during the catalytic cycle, as observed in dII upon dIII attachment/detachment (Fig. 4).

The differences between ovine and *T. thermophilus* dII are also in the P-side (intermembrane space) cavity, gated by a conserved residue E806 which in ovine dII is in an extended conformation in contrast to the *T. thermophilus* structures, with T674 and E678 allowing access to the P-side. Residues at the P-side of the proton transfer path are generally much less conserved between species than at the N-side. The P-side entry cavity in mammals also has a stronger negative charge (Extended Data Fig. 6g), appropriate for the attraction of protons in the forward reaction.

In contrast to what has been suggested for the *T. thermophilus* enzyme, dIII attachment to dII does not change the conformation of the short lateral helix CL8 nor does it disrupt the conserved salt bridge R839-D787 (Extended data Fig. 8c)[1].

Detailed explanation of the mechanism

As outlined in the main text, the excess of $NADP^+$ and pmf will promote forward reaction in the cycle shown in Fig. 5. After a full cycle and hydride transfer back at step 1, subsequent dIII dissociation from dI in step 2 is unlikely to be initiated by hydride transfer itself as it is a fast step and dI_2dIII structures were solved with many combinations of bound nucleotides[7,10]. However, NNT always operates as a dimer, in which the two dIII domains cannot simultaneously attach to the dI dimer, as noted above. Therefore, as the second monomer (in grey in Fig. 5) goes through a similar cycle as the first monomer (in colour), the second dIII, swivelling up after detachment from dII, will clash with the already bound dIII from the first monomer and dislodge it, initiating its flip "down" in step 2, resuming the cycle. This sequence of events ensures tight coupling between hydride transfer, nucleotide exchange and proton translocation. "Slipping", or uncoupling, at any step is prevented because proton translocation cannot happen without nucleotide exchange. For example, step 3 (Fig. 5) cannot progress to step 4 and switch proton channel access unless there is nucleotide exchange – only the dIII-$NADP^+$ and $H664^+$ combination will allow dIII dissociation and dII opening to the N-side. If nucleotide exchange does not happen, bound dIII-NADPH will interact strongly with $H664^+$ and prevent dIII detachment and dII opening to the N-side. In other words, two half-paths of proton across the membrane (up to H664 and after) in both forward and reverse reactions are connected only by nucleotide exchange, excluding any uncoupling.

In the reverse reaction, when pmf is low and there is an excess of NADPH, all the steps are naturally reversed, resulting in proton pumping into the P-side (Extended Data Fig. 9b). After hydride transfer, dIII-$NADP^+$ is dislodged by an incoming dIII from the opposing monomer and is attached to dII with protonated $H664^+$ (as pH is now lower in the matrix) (steps 1-2). This opens the channel to the P-side and H664 loses its proton there, as its pK_a is reduced due to interaction with $NADP^+$ (step 2). Nucleotide exchange follows due to the excess of NADPH (step 3) and dIII-NADPH swivels "up", due to its low affinity to neutral H664, back to step 1. In both forward and reverse reactions, NAD^+/NADH formed in dI in step 1 would be exchanged for NADH/NAD^+ before step 4 completes, so that the cycle can resume, since dI remains open throughout.

The proposed mechanism ensures tight coupling also close to the equilibrium conditions. We can simply consider all possibilities. After hydride transfer in step 1, dIII associates with dII, allowing nucleotide exchange. Subsequent to nucleotide exchange possible scenarios will be as follows:

1. If it is dIII-NADP+ and $H664^+$ (weak dIII-dII interaction), then dIII would be flipped up first, then dII is closed from periplasm and opened to cytoplasm, so that proton is released into the cytoplasm – this is forward reaction, when there is excess of $NADP^+$.

2. If it is dIII-$NADP^+$ and H664 (strong dIII-dII interaction), dIII will remain attached to dII until H664 is protonated from the periplasm. This prevents slipping of forward reaction. After H664 protonation dIII will be flipped up and proton released into the cytoplasm, in the forward reaction as above.

3. If it is dIII-NADPH and H664 (weak dIII-dII interaction), dIII will flip up first, then dII will close to the periplasm and open to cytoplasm, allowing H664 protonation from the cytoplasm - this is reverse reaction, when there is excess of NADPH.

4. If it is dIII-NADPH and $H664^+$ (strong dIII-dII interaction), dIII will remain attached to dII until H664 is de-protonated into the periplasm. This prevents slipping of reverse reaction. After H664 de-protonation, dIII can flip up and dII will close to the periplasm and open to cytoplasm, allowing H664 protonation from the cytoplasm, in the reverse reaction as above.

5. In the apo state, dIII remains attached to dII, preventing proton leak.

Thus, we achieve tight coupling between hydride transfer and proton translocation, without any slipping, at all conditions – either favourable for forward or reverse reaction, or close to equilibrium. Close to equilibrium the overall net direction of reaction will depend on the pmf value and nucleotide ratios.

Communication between the two monomers

The mechanism outlined above and previous biochemical data imply strong coupling between the two monomers resulting in their 'anti-phase' action. Our structures suggest different ways in which the two monomers can communicate with each other, in addition to one dIII dislodging another one from dI.

Rotation of one dIII into the face-up position (modelled on dI_2dIII crystal structures) would bring the two dIII domains much closer together than in the "double face-down" structure, so that they can form many hydrogen bonds without clashing and so interact when swivelling (Extended Data Fig. 8a).

dI dimer is stabilised by a large buried surface extended by an elongated hairpin (ovine residues 172-184) reaching out from each monomer into the neighbour[8,13,14]. The hairpin from one dI monomer interacts only weakly or not at all with the "face-down" dIII in

another monomer (as seen in our structures), but strongly with the “face-up” dIII (as in dI_2dIII crystal structures). This hairpin originates directly from the Rossmann fold coordinating the NAD(H) in the first monomer, which may allow for communication of the redox state from one dI monomer to the other.

Additionally, in mammalian enzyme the dI-dII linker contacts the dIII from one monomer and is continued by the TM1, which forms extensive interactions with the TM5 and the TM4-5 loop from another monomer, which in turn directly contact dIII from that monomer (Fig. 1d). This feature, in addition to the TM1/TM5 dimer stabilisation, may allow for more efficient dIII cross-talk. Together, all these possible routes of communication may allow for the two monomers to work more effectively in an anti-phase fashion.

Supplementary Table 1. Catalytic activities of site-directed mutants in *E. coli* NNT

Homol-ogous ovine residue	*E. coli* mutation	Reverse activity	Cyclic activity	Proton pumping activity	Notes	Structural and mechanistic explanation if conserved	Reference
D214	D195E	8%	N/A	N/A	forward activity inhibited by ~79%	part of the NAD(H)-binding pocket	[15]
Y245	Y226F	~40%	N/A	31%	~3x increase in K_m for $APAD^+$	part of the NAD(H)-binding pocket - mobile loop	[16]
Y245	Y226L	38%	N/A	13%	~3x increase for $APAD^+$	part of the NAD(H)-binding pocket - mobile loop	[16]
Y245	Y226H	45%	N/A	28-42%	~3x increase for $APAD^+$	part of the NAD(H)-binding pocket - mobile loop	[16]
Y245	Y226N	43%	N/A	51%	N/A	part of the NAD(H)-binding pocket - mobile loop	[16]
K251	D232N	45%	N/A	67%	N/A		[17]
K251	D232E	89%	N/A	110%	N/A		[17]
K251	D232K	75%	N/A	65%	N/A		[17]
K251	D232H	84%	N/A	98%	N/A		[17]
E257	E238Q	71%	N/A	18%	N/A	part of the NAD(H)-binding pocket	[17]
E257	E238K	41%	N/A	27%	N/A	part of the NAD(H)-binding pocket	[17]
K259	E240Q	N/A	N/A	N/A	3x increased K_m for $APAD^+$ but not for NADH		[17]
	triple D232N E238Q E240Q	55%	N/A	59%	lower inhibition by DCCD than wt, both in the presence and absence of NAD(P)H		[17]
	triple D232H E238Q E240Q	44%	N/A	51%	lower inhibition by DCCD than wt, both in the presence and absence of NADH(P)H		[17]
A454	E423C	>75%	N/A	N/A			[18]
Y470	Y439F	41%	N/A	38%		part of the lipid binding pocket at the dimer interface	[19]
A479	A448C	50-75%	N/A	N/A		part of the dII-dIII interface	[18]
H481	H450T	17%	N/A	51%	Greatly lowered activity but still pumps protons	part of the dII-dIII interface	[20]
H481	H450T	26%	3000%	21%		part of the dII-dIII interface	[21]
T488	T457A	80%	N/A	109%		immediate vicinity to the proton pumping residue N489	[19]
N489	N458A	66%	N/A	44%		part of the proton pumping machinery	[19]
S492	S461	51%	N/A	67%		immediate vicinity to the proton pumping residue N489	[19]
	triple T457A N458A S461A	9%	N/A	22%			[19]
G505	Q474C	>75%	N/A	N/A			[18]
L507	G476C	93%	81%	N/A	double mutants with cysteines on other cytoplasmic loops generated and cross-linked; activities were mainly preserved (above 50%)		[22]
N527	N492A	54%	N/A	78%		immediate vicinity to the proton pumping residue N489	[19]
L533	T498C	>75%	N/A	N/A			[18]
T535	T500A	49%	N/A	56%		not part of proton transfer pathway	[19]
Q536	Q501C	>75%	N/A	N/A		not part of proton transfer pathway	[18]
R537	R502S	71%	N/A	93%		not part of proton transfer pathway	[17]
540-545	Δ(505-510)	6%	371%	N/A	$NADP^+$ independent cyclic activity increased by 35x - enzyme co-purifies with $NADP^+$ at 0.2 mol/mol	CL2 (esp. R544) is important for dII-dIII interface formation, deletion of this loop locks the enzyme in the dIII-detached state, explaining the copurification with NADP+, increased cyclic activity and decreased	[23]

						reverse activity, because NADP(H) cannot exchange without dIII interacting with dII	
543-545	Δ(508-510)	50%	253%	N/A	$NADP^+$ independent cyclic activity increased by 306%	CL2 (esp. R544) is important for dII-dIII interface formation, deletion of this loop locks the enzyme in the dIII-detached state, explaining the increased cyclic activity and decreased reverse activity, because NADP(H) cannot exchange without dIII interacting with dII	23
R544	K509E	50%	201%	N/A	$NADP^+$ independent cyclic activity increased by 168%	R544 important for dII-dIII interface formation, mutation of this residue locks the enzyme in the dIII-detached state, explaining the increased cyclic activity and decreased reverse activity, because NADP(H) cannot exchange without dIII interacting with dII	23
G573	S2C	100%	95%	N/A			18,22
L595	L24C	~15%	N/A	N/A		not part of proton transfer pathway, buried residue	18
A601	S30C	>75%	N/A	N/A			18
R602	R31A	19%	8%	8%		stabilises CL3, TM5 and TM6	24
R602	R31E	>120%	61%	>120%		stabilises CL3, TM5 and TM6	24
R602	R31L	41%	15%	46%		stabilises CL3, TM5 and TM6	24
N605	N34A	59%	N/A	79%		not part of proton transfer pathway	19
N605	N34T	>120%	92%	>120%		not part of proton transfer pathway	24
P627	T54C	50% or >75%	65%	N/A			18,22
K649	K76Q	99%	95%	~100%		not part of proton transfer pathway	24
R650	K77A	9%	4%	11%			24
R650	K77L	13%	4%	19%			24
R650	K77Q	49%	46%	62%			24
S654	T81C	50-75%	N/A	N/A			18
D655	E82K	79%	N/A	66%			20
D655	E82Q	63% or 49%	N/A	85% or 63%			19,20
Q658	E85A	9%	19%	9%		N-terminal part of the TM9 which undergoes changes during dIII attachment	24
Q658	E85C	4% or 50-75	3%	8%		N-terminal part of the TM9 which undergoes changes during dIII attachment	18,24
Q658	E85K	15%	4%	14%		N-terminal part of the TM9 which undergoes changes during dIII attachment	24
Q658	E85L	8%	5%	7%		N-terminal part of the TM9 which undergoes changes during dIII attachment	24
Q658	E85Q	3% or 63%	2%	4% or 71%		N-terminal part of the TM9 which undergoes changes during dIII attachment	19,24
Q658	E85S	22%	6%	20%		N-terminal part of the TM9 which undergoes changes during dIII attachment	24
	triple E79Q E82Q E85Q	55%	N/A	94%			19
H664	H91A	7%	10%	0%	H664 is a key residue for proton translocation and based on its protonation state stabilises face-down dIII-$NADP^+$ or dIII-NADPH	Mutation to small and nonpolar residue stabilised NNT in a face-down conformation, hence no cyclic or reverse activity measurable	24
H664	H91C	12% or 3% or 24%	11%	7% or 0% or 0%	No conformational change in β chain induced by NADP(H) binding - as measured by βR265 susceptibility to trypsin	Mutation to small and uncharged residue stabilised NNT in a face-down conformation, hence no cyclic or reverse activity measurable and NADP(H) cannot induce change of conformations	20,24,25
H664	H91D	9% or 25%	240% or 12%	6% or 0%		Cyclic activity data conflicting; NNT could be trapped either in dIII-attached or detached conformations; based on H91E mutation, dIII-attached conformation is more likely	24,26
H664	H91E	15%	3%	0%		Negatively charged residue stabilised NNT in a face-down conformation; hence no cyclic or reverse activity	24
H664	H91G	27%	15%	0%		Mutation to small and uncharged residue stabilised NNT in a face-down conformation, hence radically reduced cyclic or reverse activities	24
H664	H91I	28%	6%	2%		Mutation to nonpolar residue stabilised NNT in a face-down conformation, hence radically reduced cyclic	24

						and reverse activities	
H664	H91L	18%	11%	2%		Mutation to nonpolar residue stabilised NNT in a face-down conformation, hence radically reduced cyclic and reverse activities	24
H664	H91K	4% or 2% or 5% or 4%	260% or 120% or 3-20%	20% or 30% or 1%	Also increases $NADP^+$ independent cyclic activity by 40x - copurifies with 0.2 mol $NADP^+$ per mol; present in NADP(H) induced conformation as shown by susceptibility to trypsinolysis at βR265; Measured at large nucleotide conc. (0.5mM NADPH, 1mM APAD for reverse; 1mM NADH or 0.5mM $NADP^+$ and NADH each);	positive charge on H91 promotes dissociation of dIII- $NADP^+$, hence increased cyclic activity and co-purification with $NADP^+$; substitution for a bulky Lys at this crucial site prevents NADP(H) insertion and locks dII in the detached state	23–27
H664	H91M	16%	3%	<1%		Mutation to nonpolar residue stabilised NNT in a face-down conformation, hence radically reduced cyclic and reverse activities	24
H664	H91N	80% or 86% or 66% or 18%	8% or 44%	7% or 0% or 0% or 7% or 4%	Proton transfer activity is inhibited	NNT trapped in the face-down conformation; Asn cannot be protonated, hence complete inhibition of proton transfer and reduced reverse/cyclic activities as detachment of dIII is dysregulated	21,24–26
H664	H91R	1% or 7%	228% or 8%	25% or 0%	pH dependence of reverse activity disrupted - shifted towards acidic pH, pH dependence of cyclic activity stays the same; retains 0.8 mol NADP(H) per dimer	consistent with H91K mutant: positive charge on H91 promotes dissociation of dIII- $NADP^+$, hence increased cyclic activity and co-purification with $NADP^+$; NADP(H) cannot insert into dII stabilised in N-side open state	26
H664	H91S	19% or 6%	N/A	11% or 8%	No conformational change in β chain induced by NADP(H) binding - as measured by βR265 susceptibility to trypsin	Mutation to small and uncharged residue stabilised NNT in a face-down conformation; hence no reverse activity measurable and NADP(H) cannot induce change of conformations	20,25
H664	H91T	11% or 2%	N/A	8% or 8%	No conformational change in β chain induced by NADP(H) binding - as measured by βR265 susceptibility to trypsin	Mutation to small and uncharged residue stabilised NNT in a face-down conformation; hence no reverse activity measurable and NADP(H) cannot induce change of conformations	20,25
H664	H91V	17%	3%	0%		Mutation to small and non-polar residue stabilised NNT in a face-down conformation; hence no cyclic or reverse activity measurable and NADP(H) cannot induce change of conformations	24
H664	H91W	3%	3%	0%		Bulky residue stabilised dII in a dIII-attached state, hence no reverse and cyclic activities	24
H664	H91Y	7%	8%	1%		Bulky residue stabilised dII a dIII-attached state, hence no reverse and cyclic activities	24
S665	S92A	>120% or 53%	95%	>120% or 78%		not part of proton transfer pathway	19,24
S665	S92C	>75%	N/A	N/A		not part of proton transfer pathway	18
G668	G95A	56%	45%	44%	no cyclic activity without NADPH; rev. act measured at 200 μM substrates, cyclic at 10 μM NADPH	not part of proton transfer pathway	28
E678	S105C	37% or >75%	85%	N/A			18,22
I681 E682	double H108N H109N	51%	N/A	69%			19
E682-F685	deltaH109-G112	58%	49%	N/A	β domain was split into two my introducing a stop codon at H109		29
T688	A114C	~15%	N/A	N/A			18
V698	E124C	15%	>100%	N/A	pH dependence of reverse activity shifted toward acidic - max. rate at pH6		22
V698	E124K	46%	30%	36%			24
V698	E124A	28%	68%	41%			24
V698	E124Q	41%	N/A	150%			19
G706	G132A	101%	70%	101%	no cyclic activity without NADPH; rev. act measured at 200 μM substrates, cyclic at 10 μM NADPH	not part of proton transfer pathway	28
T709	T135A	73%	52%	31%		not part of proton transfer pathway but in close vicinity to be able to distort local environment	24
T709	T135C	55%	13%	16%		not part of proton transfer pathway but in close vicinity to be able to distort local environment	24

T709	T135D	71%	6%	28%		not part of proton transfer pathway but in close vicinity to be able to distort local environment	[24]
T709	T135K	5%	100%	1%		not part of proton transfer pathway but in close vicinity to be able to distort local environment; bulky residue could stabilise detached dII, giving rise to retained cyclic activity	[24]
T709	T135L	33%	77%	9%		not part of proton transfer pathway but in close vicinity to be able to distort local environment; bulky residue could stabilise detached dII, giving rise to retained cyclic activity	[24]
T709	T135S	23%	17%	12%		not part of proton transfer pathway but in close vicinity to be able to distort local environment	[24]
S711	T137A	100-120%	70%	100-120%		not part of proton transfer pathway	[24]
G712	G138A	57%	34%	32%	no cyclic activity without NADPH; rev. act measured at 200 μM substrates, cyclic at 10 μM NADPH	not part of proton transfer pathway	[28]
S713	S139A	6%	12%	0%		not part of proton transfer pathway but in close vicinity to be able to distort local environment	[24]
S713	S139C	34%	63%	33%		not part of proton transfer pathway but in close vicinity to be able to distort local environment	[24]
S713	S139D	2%	4%	0%		not part of proton transfer pathway but in close vicinity to be able to distort local environment	[24]
S713	S139G	83%	31%	41%		not part of proton transfer pathway but in close vicinity to be able to distort local environment	[24]
S713	S139H	1%	2%	0%		not part of proton transfer pathway but in close vicinity to be able to distort local environment	[24]
S713	S139K	2%	4%	0%		not part of proton transfer pathway but in close vicinity to be able to distort local environment	[24]
S713	S139L	4%	6%	0%		not part of proton transfer pathway but in close vicinity to be able to distort local environment	[24]
S713	S139N	3%	3%	0%		not part of proton transfer pathway but in close vicinity to be able to distort local environment	[24]
S713	S139T	96%	77%	71%		not part of proton transfer pathway but in close vicinity to be able to distort local environment	[24]
S713	triple T135A T137A S139A	29%	N/A	155%			[19]
A716	A142C	>75%	N/A	N/A		not part of proton transfer pathway but in close vicinity to be able to distort local environment	[18]
K719	K145A	44%	21%	50%		Important for maintaining integrity of dII (stabilises CL6 by salt bridge to the main chain), hence inhibition of all activities	[24]
K719	K145E	46%	57%	67%		Important for maintaining integrity of dII (stabilises CL6 by salt bridge to the main chain), hence inhibition of all activities	[24]
K719	K145L	19%	23%	2%		Important for maintaining integrity of dII (stabilises CL6 by salt bridge to the main chain), hence inhibition of all activities	[24]
K719	K145T	29%	N/A	71%		Important for maintaining integrity of dII (stabilises CL6 by salt bridge to the main chain), hence inhibition of all activities	[19]
I723	K149Q	49%	58%	67%			[24]
A727	K153A	17%	16%	19%			[24]
A727	K153Q	50%	60%	7%			[24]
L731	A157C	>75%	N/A	N/A			[18]
R734	R160A	45%	18%	3%		Important for maintaining integrity of dII (stabilises CL6 by salt bridge to the main chain of CL8), hence inhibition of all activities	[24]
R734	R160L	97%	40%	68%		Important for maintaining integrity of dII (stabilises CL6 by salt bridge to the main chain of CL8), hence inhibition of all activities	[24]
H735	H161S	90%	N/A	100%		not part of proton transfer pathway or structurally important	[20]
H735	H161T	88% or 98%	122%	108 or 110%		not part of proton transfer pathway or structurally important	[20,21]
H735	H161C	59%	N/A	94%	Little effect	not part of proton transfer pathway or structurally important	[20,21]
N738	N164T	>120%	>120%	100-120%		not part of proton transfer pathway or structurally important	[24]
G747	L173C	50-75%	N/A	N/A			[18]
S757	S183C	50% or	65%	N/A		faces the IMS, no catalytic role	[18,22]

		>75%					
S767	I193C	N/A	N/A	N/A		no catalytic role	[18]
A782	S208C	>75%	N/A	N/A			[18]
D787	D213A	13%	14%	4%		Important for integrity of dII and transmission of conformational changes between dII and dIII (stabilises CL7 and CL8 by salt bridge to R839); mutant stabilised in face-down state and all the activities were inhibited	[24]
D787	D213E	34% or 20%	28%	77% or 18%		Mutation to a similar residue gives a milder but noticeable phenotype	[24,26]
D787	D213G	2%	3%	0%		Important for integrity of dII and transmission of conformational changes between dII and dIII (stabilises CL7 and CL8 by salt bridge to R839); mutant stabilised in face-down state and all the activities were inhibited	[24]
D787	D213H	82%	N/A	34%		Mutation to a similar residue gives a milder but noticeable phenotype	[20]
D787	D213I	11%	62%	N/A	Decreased K_m(NADPH) from 33 μM to 9.1 μM; decreased $S_{0.5}$ for NADPH from 2.7 to 0.27 μM in cyclic reaction	Important for integrity of dII and transmission of conformational changes between dII and dIII (stabilises CL7 and CL8 by salt bridge to R839); mutant stabilised in dIII-detached state as suggested by decreased K_m(NADPH) and less affected cyclic activity	[30]
D787	D213K	7% or 4%	8%	49% or 5%		Important for integrity of dII and transmission of conformational changes between dII and dIII (stabilises CL7 and CL8 by salt bridge to R839); mutant stabilised in face-down state and all the activities were inhibited	[24,26]
D787	D213N	23% or 92%	67%	44%	Decreased K_m(NADPH) from 33 μM to 20 μM; decreased $S_{0.5}$ for NADPH from 2.7 to 0.43 μM in cyclic reaction	Important for integrity of dII and transmission of conformational changes between dII and dIII (stabilises CL7 and CL8 by salt bridge to R839); mutant stabilised in dIII-detached state as suggested by decreased K_m(NADPH) and less affected cyclic activity	[20,30]
D787	D213L	4%	6%	3%		Important for integrity of dII and transmission of conformational changes between dII and dIII (stabilises CL7 and CL8 by salt bridge to R839); mutant stabilised in face-down state and all the activities were inhibited	[24]
D787	D213R	5%	33%	28% or 6%		Important for integrity of dII and transmission of conformational changes between dII and dIII (stabilises CL7 and CL8 by salt bridge to R839); mutant stabilised in face-down state and all the activities were inhibited	[24,26]
D787	double D213N E82Q	25%	N/A	81%			[19]
M788	M214C	50-75%	N/A	N/A		part of CL7 and in close vicinity to dII-dIII interface	[18]
V790	V216C	50-75%	N/A	N/A		close vicinity to proton translocation pathway	[18]
T793	S219A	100%	>120%	>120%		close vicinity to proton translocation pathway	[24]
T793	S219C	50-75%	N/A	N/A		close vicinity to proton translocation pathway	[18]
N796	N222A	18% or 9%	17% or 4%	0% or 10%		part of proton translocation pathway; mutation to a small nonpolar residue stabilises the face-down dIII conformation, hence inhibition of all activities	[19,24,26]
N796	N222C	58% or 48%	59% or 24%	11% or 30%		part of proton translocation pathway, hence proton transfer activity affected the strongest; mutation to a small uncharged residue also stabilises the face-down dIII conformation, hence intermediate inhibition of reverse and cyclic activities as well	[19,24,31]
N796	N222D	13% or 21% or 15%	100% or 23% or 7%	22% or 13% or 14%		Not entirely consistent measurements, introduction of negative charge at N796 appears to favour dIII-attached conformation and favours face-down dIII	[19,24,26]
N796	N222G	2% or 11%	2% or 5%	0% or 10%		part of proton translocation pathway; mutation to a small nonpolar residue stabilises the face-down dIII conformation, hence inhibition of all activities	[24,31]
N796	N222H	7% or 35% or 12%	114% or 18% or 4%	7% or 0% or 4%		Different measurements not entirely consistent; N796 part of proton translocation pathway, hence proton transfer activity affected the strongest; mutation to a small uncharged residue also stabilises the face-down dIII conformation, hence intermediate inhibition of reverse and cyclic activities as well	[19,24,26]
N796	N222K	3% or 11%	15%	13% or 0%	retains 0.58 mol of NADP(H) per dimer	Part of proton translocation pathway next to H664; confirms observations on H91K/R mutants; low cyclic	[24,26]

						activity not entirely consistent	
N796	N222L	52%	28%	1%		Part of proton translocation pathway next to H664; mutation to a nonpolar residue stabilises the face-down dIII conformation, hence inhibition of all activities	24
N796	N222Q	15%	16%	0%		Part of proton translocation pathway next to H664; introduction of a larger residue stabilises the face-down dIII conformation, hence inhibition of all activities	24
N796	N222R	2% or 2% or 3%	214% or 9% or 57%	13% or 0% or 11%	retains 0.44 mol of NADP(H) per dimer	Part of proton translocation pathway next to H664; confirms observations on H91K/R mutants: dIII-detached NNT copurifies with NADP(H) and catalyses cyclic reaction	19,24,26
N796	N222S	3%	1%	0%		Part of proton translocation pathway next to H664; mutation to a nonpolar residue stabilises the face-down dIII conformation, hence inhibition of all activities	24
N796	N222Y	3% or 3%	7% or 3%	0% or 6%		Part of proton translocation pathway next to H664; mutation stabilises the face-down dIII conformation, hence inhibition of all activities	19,24
N796, H664	double N222H H91N	2%	N/A	8%		part of proton translocation pathway, mutant stabilised in face-down dIII conformation, underlines the sensitivity of this area to small changes	26
S797	S223A	>120%	>120%	>120%		not part of proton transfer pathway but in close enough vicinity to be able to distort local environment	24
Y798	Y224F	83% or 49%	>120% or 93%	95% or 92%		not part of proton transfer pathway but in close enough vicinity to be able to distort local environment	24,31
Y798	double Y224F N222A	8%	5%	10%		not part of proton transfer pathway but in close enough vicinity to be able to distort local environment	19
S799	S225A	87%	88%	57%		consistent with S799 participating in proton translocation as the proton translocation activity is inhibited more than hydride transfer activity in the mutant enzyme	24
S799	S225C	~30%	N/A	N/A		consistent with S799 participating in proton translocation as the proton translocation activity is inhibited more than hydride transfer activity in the mutant enzyme	18
S799, S797	double S223A S225A	107%	N/A	101%		close vicinity to proton translocation pathway	19
G800	G226A	50%	70%	32%	no cyclic activity without NADPH; rev. act measured at 200 μM substrates, cyclic at 10 μM NADPH	close vicinity to proton translocation pathway	28
G807	G233A	49%	31%	30%	no cyclic activity without NADPH; rev. act measured at 200 μM substrates, cyclic at 10 μM NADPH	close vicinity to proton translocation pathway	28
N811	S237C	81% or >75%	>100%	N/A		part of IL7	18,22
N812	N238A	62%	N/A	100%		part of IL7	19
N812	N238C	50%	100%	N/A		part of IL7	32
N813	D239C	10% or 50-75%	70%	N/A			18,32
L814	L240C	40%	120%	N/A		close vicinity to proton translocation pathway and part of TMH14 important for transmitting dIII-induced changes in dII	32
L815	L241C	40%	60%	N/A		close vicinity to proton translocation pathway and part of TMH14 important for transmitting dIII-induced changes in dII	32
T816	I242C	0%	0%	N/A			32
I817	V243C	30%	40%	N/A			32
V818	T244C	40%	30%	N/A			32
G819	G245C	25%	0%	N/A		close vicinity to proton translocation pathway	32
G819	G245L	20%	50%	N/A		close vicinity to proton translocation pathway	32
G819	G245A	104%	58%	100%		close vicinity to proton translocation pathway	28
A820	A246C	140%	170%	N/A		close vicinity to proton translocation pathway	32

L821	L247C	30%	200%	N/A		close vicinity to proton translocation pathway	[32]
I822	V248C	40%	170%	N/A			[32]
G823	G249A	79%	71%	77%		close vicinity to proton translocation pathway	[28]
G823	G249C	40%	0%	N/A		close vicinity to proton translocation pathway	[32]
G823	G249L	70%	50%	N/A		close vicinity to proton translocation pathway	[32]
S824	S250A	>120%	>120%	>120%		close vicinity to proton translocation pathway	[24]
S824	S250C	250% or >75%	170%	N/A	Cyclic activity sensitive to phosphatase treatment	close vicinity to proton translocation pathway	[18,32]
S825	S251A	>120%	>120%	77%		close vicinity to proton translocation pathway	[24]
S825	S251C	130%	250%	N/A	Cyclic activity sensitive to phosphatase treatment	close vicinity to proton translocation pathway	[32]
S825	double S250A S251A	95%	N/A	115%		close vicinity to proton translocation pathway	[19]
G826	G252A	2.6%	96%	0%	Also increases $NADP^+$ independent cyclic activity by 20x – because NADPH remains bound to enzyme; measured both in membranes and purified NNT	direct contact with N796; substitution with any bulkier residue distorts the proton translocation pathway and prevents binding of dIII; consistent with co-purification with NADP(H) and high cyclic activity	[28]
G826	G252C	1.9%	85%	1.6%	Also increases $NADP^+$ independent cyclic activity by 20x – because NADPH remains bound to enzyme; measured both in membranes and purified NNT; Karlsson report lower (~20% cyclic activity)	direct contact with N796; substitution with any bulkier residue distorts the proton translocation pathway and prevents binding of dIII; consistent with co-purification with NADP(H) and high cyclic activity	[28,32]
G826	G252S	2.4%	83%	1%	Also increases $NADP^+$ independent cyclic activity by 20x – because NADPH remains bound to enzyme; measured both in membranes and purified NNT	direct contact with N796; substitution with any bulkier residue distorts the proton translocation pathway and prevents binding of dIII; consistent with co-purification with NADP(H) and high cyclic activity	[28]
G826	G252T	2.3%	101%	0%	Also increases $NADP^+$ independent cyclic activity by 20x – because NADPH remains bound to enzyme; measured both in membranes and purified NNT	direct contact with N796; substitution with any bulkier residue distorts the proton translocation pathway and prevents binding of dIII; consistent with co-purification with NADP(H) and high cyclic activity	[28]
G826	G252V	2.5%	22%	0%	Also increases $NADP^+$ independent cyclic activity by 4.5x – because NADPH remains bound to enzyme	direct contact with N796; substitution with any bulkier residue distorts the proton translocation pathway and prevents binding of dIII; consistent with co-purification with NADP(H) and high cyclic activity	[28]
G826	G252L	10%	20%	N/A		direct contact with N796; substitution with any bulkier residue distorts the proton translocation pathway and prevents binding of dIII; consistent with co-purification with NADP(H) and high cyclic activity	[32]
A827	A253C	50%	150%	N/A		close vicinity to proton translocation pathway	[32]
I828	I254C	30%	100%	N/A		close vicinity to proton translocation pathway	[32]
L829	I255C	80%	150%	N/A			[32]
S830	S256A	89%	>120%	95%		close vicinity to proton translocation pathway	[24]
S830	S256C	220%	150%	N/A	Cyclic activity sensitive to phosphatase treatment	close vicinity to proton translocation pathway	[32]
Y831	Y257F	>120%	>120%	>120%		close vicinity to proton translocation pathway	[24]
Y831	Y257C	70%	120%	N/A		close vicinity to proton translocation pathway	[32]
Y831	double S256A Y257F	88%	N/A	69%		close vicinity to proton translocation pathway	[19]
I832	I258C	70%	80%	N/A		important in switching dII between the two conformations; mutant switches more slowly	[32]
M833	M259C	20%	220%	N/A	Cyclic activity not sensitive to phosphatase treatment	important in switching dII between the two conformations; mutant locked in dIII-detached conformation	[32]
C834	S260C	44% or 78% or 250%	130% or 100%	57%	No increase of $NADP^+$ independent cyclic activity; Karlsson et al 2003 report enchanced reverse transhydrogenation activity	Measurements not entirely consistent; this residue is important in switching dII between the two conformations	[20,23,32]
C834	S260C	23%	~50%	N/A	done in cysteine-free NNT	important in switching dII between the two conformations	[33]
V835	K261C	8%	~40%	N/A	done in cysteine-free NNT		[33]

A836	A262C	8% or 50-75%	~60%	N/A	done in cysteine-free NNT; also measured labelling of this cysteine by a maleimide MIANS; stimulated by $NADP^+$ and to a lesser degree NADPH addition	important in switching dII between the two conformations; mutant slightly stabilised in dIII-detached conformation based on cyclic activity	[18,33]
M837	M263C	5%	~50%	N/A	done in cysteine-free NNT	important in switching dII between the two conformations; mutant slightly stabilised in dIII-detached conformation based on cyclic activity	[33]
N838	N264C	10%	~30%	N/A	done in cysteine-free NNT	important in switching dII between the two conformations; mutant slightly stabilised in dIII-detached conformation based on cyclic activity	[33]
R839	R265C	8%	100%	N/A	3x higher $NADP^+$ independent cyclic activity, paradoxically increased K_m for NADPH from 7 μM to 17 μM; done in cysteine-free NNT; pH optimum for reverse reaction shifted towards acidic pH (~6.5)	Maintains integrity of dII and transmits conformational changes between dII and dIII; mutant locked in dIII-detached conformation, hence reverse activity inhibited more than cyclic activity	[33]
R839	R265A	20%	~150%	N/A	pH optimum for reverse reaction shifted towards acidic pH (~6.5)	Maintains integrity of dII and transmits conformational changes between dII and dIII; mutant locked in dIII-detached conformation, hence reverse activity inhibited more than cyclic activity	[33]
R839	R265E	8%	~90%	N/A	pH optimum for reverse reaction shifted towards acidic pH (~6.5)	Maintains integrity of dII and transmits conformational changes between dII and dIII; mutant locked in dIII-detached conformation, hence reverse activity inhibited more than cyclic activity	[33]
R839	R265K	34%	~130%	N/A	pH optimum for reverse reaction shifted towards acidic pH (~6.5)	Maintains integrity of dII and transmits conformational changes between dII and dIII; mutant locked in dIII-detached conformation, hence reverse activity inhibited more than cyclic activity	[33]
R839	R265C AND D213C	5%	~30%	N/A	NADP(H)-independent cyclic activity N/A; done in cysteine-free NNT;	Maintains integrity of dII and transmits conformational changes between dII and dIII; mutant locked in dIII-detached conformation, hence reverse activity inhibited more than cyclic activity	[33]
S840	S266C	69%	~90%	N/A	2.4x higher $NADP^+$ independent cyclic activity, K_m for NADPH 5.3 μM	not part of catalytic machinery	[33]
G848	G274A	72%	45%	N/A		not part of catalytic machinery	[34]
G848	G274D	50%	63%	N/A		not part of catalytic machinery	[34]
G848	G274V	57%	39%	N/A		not part of catalytic machinery	[34]
G850	G276A	60%	42%	N/A		not part of catalytic machinery	[34]
G850	G276V	40%	16%	N/A		not part of catalytic machinery	[34]
G850	G276F	41%	29%	N/A		not part of catalytic machinery	[34]
G889	G314A	7% or 4%	3% or 0%	N/A	No increase of $NADP^+$ independent cyclic activity; trypsinolysis of β subunit not stimulated by NADP(H)	part of the NADP(H) binding pocket, mutation prevents NADP(H) binding, hence all activities inhibited	[23,34,35]
G889	G314E	1%	0%	0%	spontaneous mutation in E. coli RH1 strain; trypsinolysis of β subunit not stimulated by NADP(H)	part of the NADP(H) binding pocket, mutation prevents NADP(H) binding, hence all activities inhibited	[34–36]
G889	G314C	1%	0%	N/A	trypsinolysis of β subunit not stimulated by NADP(H)	part of the NADP(H) binding pocket, mutation prevents NADP(H) binding, hence all activities inhibited	[34,35]
G889	G314V	1%	0%	N/A	trypsinolysis of β subunit not stimulated by NADP(H)	part of the NADP(H) binding pocket, mutation prevents NADP(H) binding, hence all activities inhibited	[34,35]
Y890	Y315H	28%	N/A	63%		part of the NADP(H) binding pocket, also involved in opening of dIII	[16]
Y890	Y315I	4%	N/A	N/A		part of the NADP(H) binding pocket, also involved in opening of dIII	[16]
Y890	Y315F	62%	N/A	60%	Phe mutant 50% activity and pumps protons	part of the NADP(H) binding pocket, also involved in opening of dIII	[16]
Y890	Y315D	6%	N/A	N/A		part of the NADP(H) binding pocket, also involved in opening of dIII	[16]
Y890	Y315N	25%	N/A	20%		part of the NADP(H) binding pocket, also involved in opening of dIII	[16]
Y890	Y315V	4%	N/A	N/A		part of the NADP(H) binding pocket, also involved in opening of dIII	[16]
Y890	Y315L	13	N/A	N/A		part of the NADP(H) binding pocket, also involved in opening of dIII	[16]
A894	V319G	55%	N/A	N/A	trypsinolysis pattern the same as wild-type		[34]
G912	G337A	68%	N/A	N/A	trypsinolysis pattern the same as wild-type	not part of catalytic machinery	[34]
G912	G337D	95%	N/A	N/A	trypsinolysis pattern the same as wild-type	not part of catalytic machinery	[34]
G912	G337E	93%	N/A	N/A	trypsinolysis pattern the same as wild-type	not part of catalytic machinery	[34]

G912	double V319G G337D	11%	N/A	N/A	trypsinolysis pattern the same as wild-type	not part of catalytic machinery	[34]
H920	H345C	250%	N/A	26%	done in isolated dIII; retains less NADP(H)	very close to the NADP(H) binding site, destabilises nucleotide binding, making exchange possible even when not bound to dII, hence decoupled phenotype	[37]
H920	H345N	8% or 7%	830%	12%	additional trypsin fragment of β subunit; NADP(H)-stimulated β subunit cleavage still present	very close to the NADP(H) binding site, stimulates nucleotide binding, hence high cyclic and low reverse activities	[21,34]
H920	H345Q	18% or 17%	22%	30%	additional trypsin fragment of β subunit; NADP(H)-stimulated β subunit cleavage still present	very close to the NADP(H) binding site, slows down nucleotide exchange inhibiting all activities	[21,34]
	double G337D H345Q	5%	N/A	N/A	fully cleaved in the absence of substrates		[34]
	triple V319G G337D H345Q	1%	N/A	N/A			[34]
A923	A348C	825%	N/A	67%	done in isolated dIII; retains 60% NADPH, 34% in apo form	part of the NADP(H) binding pocket, destabilises nucleotide binding, making exchange possible even when not bound to dII, hence decoupled phenotype	[37]
R925	R350C	250% or 4%	7%	41%	done in isolated dIII; 24% with $NADP^+$, 30% with NADPH, 46% in apo form	part of the NADP(H) binding pocket, coordinates diphosphate; NADP(H) binding is destabilised and exchange possible even when not bound to dII, hence decoupled phenotype	[34,37]
R925	R350S	4%	1%	N/A		part of the NADP(H) binding pocket, coordinates diphosphate; NADP(H) binding is destabilised in mutant	[34]
R925	R350G	5%	0%	N/A		part of the NADP(H) binding pocket, coordinates diphosphate; NADP(H) binding is destabilised in mutant	[34]
R925	double H345Q R350G	1%	N/A	N/A	fully cleaved in the absence of substrates	Trapped in dIII-detached conformation without the nucleotide bound	[34]
R925	triple V319G H345Q R350G	1%	N/A	N/A	fully cleaved in the absence of substrates	Trapped in dIII-detached conformation without the nucleotide bound	[34]
R925	triple G337D H345Q R350G	0%	N/A	N/A	fully cleaved in the absence of substrates	Trapped in dIII-detached conformation without the nucleotide bound	[34]
R925	quadruple V319G G337D H345Q R350G	1%	N/A	N/A	fully cleaved in the absence of substrates	Trapped in dIII-detached conformation without the nucleotide bound	[34]
Q929	H354Q	10%	78%	10%			[21]
Q929	H354Y	11%	11%	11%			[21]
E936	E361Q	20%	40%	113%		at the edge of the dII-dIII interface, stabilising effect on the interface, such that its formation is not strictly controlled by the nucleotide exchange, hence decoupled phenotype	[38]
E946	E371Q	71%	78%	34%		at the edge of the dII-dIII interface	[38]
E949	E374L	63%	708%	33%		not part of catalytic machinery; stabilises dIII in the detached state	[38]
D958	D383L	49%	79%	N/A		not part of catalytic machinery	[38]
D958	D383R	92%	123%	N/A		not part of catalytic machinery	[38]
A965	A390C	74%	106%	N/A		close to the NADP(H) binding site but facing away from it	[37]
D967	D392C	1375%	N/A	18%	done in isolated dIII, fully in apo form	part of the NADP(H) binding site, also contributes to stabilisation of loop E in the closed conformation, hence nucleotide exchange possible without interaction with dII and reverse activity is elevated	[37]
E967	D392A	1%	0%	44%		part of the NADP(H) binding site, prevents closing of loop E and binding of nucleotide	[38]
E967	D392K	3%	0%	2%		part of the NADP(H) binding site, prevents closing of loop E and binding of nucleotide	[38]
E967	D392N	2%	0%	13%		part of the NADP(H) binding site, prevents closing of loop E and binding of nucleotide	[38]
E967	D392Q	3%	0%	2%		part of the NADP(H) binding site, prevents closing of loop E and binding of nucleotide	[38]
E967	D392T	2%	0%	2%		part of the NADP(H) binding site, prevents closing of loop E and binding of nucleotide	[38]
T968	T393C	175%	N/A	49%	in isolated dIII; 34% $NADP^+$, 66% NADPH; 2x faster release rate of NADPH	part of the NADP(H) binding site, hydrogen bonding with diphosphate; mutation allows nucleotide exchange to be decoupled from proton transfer, hence decoupled phenotype	[39]

A973	A398C	100%	102%	N/A	in isolated dIII; forward reaction rate increased 3-fold	not part of catalytic machinery	[40]
D976	D401G	0-102%	3-76%	0-88%		part of D loop, stabilises dI-dII linker in the face-down state	[27]
D976	D401E	0-102%	3-76%	0-88%		part of D loop, stabilises dI-dII linker in the face-down state	[27]
D976	D401V	0-102%	3-76%	0-88%		part of D loop, stabilises dI-dII linker in the face-down state	[27]
S979	S404C	75%	100%	N/A	in isolated dIII; forward reaction rate increased 2-fold	part of D loop, not part of catalytic machinery	[40]
I981	S406C	450%	29%	N/A	in isolated dIII; forward reaction rate increased 35-fold; 4x faster NADPH release		[40]
G983	G408C	100%	29%	N/A	in isolated dIII; forward reaction rate increased 3-fold	surface-exposed residue, not part of catalytic machinery	[40]
M984	M409C	75%	24%	N/A	in isolated dIII; forward reaction rate increased 3-fold	close to the NADP(H) binding site	[40]
V986	V411C	125%	31%	N/A	in isolated dIII; forward reaction rate increased 5-fold	not part of catalytic machinery	[40]
E988	E413G	70-106%	N/A	89-99%		surface-exposed residue, not part of catalytic machinery	[27]
E988	E413D	70-106%	N/A	89-99%		surface-exposed residue, not part of catalytic machinery	[27]
E988	E413V	70-106%	N/A	89-99%		surface-exposed residue, not part of catalytic machinery	[27]
K991	K416G	33%	27%	82%		surface-exposed residue, not part of catalytic machinery	[27]
K999	K424C	425% - dI-dIII only; 30% full NNT	50% full NNT, 45% dI/dIII	45%	in isolated dIII; 63% apo form	part of the KRS motif of the NADP(H) binding pocket; accelerates nucleotide exchange in dI-dIII, hence faster reverse reaction but disrupts binding of NADP(H), hence slower activities measured in the full NNT	[37]
K999	K424G	1-5%	7-36%	0%		KRS motif of the NADP(H) binding pocket; disrupted nucleotide binding	[27]
K999	K424R	1-5%	7-36%	100%		KRS motif of the NADP(H) binding pocket; disrupted nucleotide binding	[27]
R1000	R425G	0-13%	1-38%	0-98%		KRS motif of the NADP(H) binding pocket; disrupted nucleotide binding	[27]
R1000	R425E	0-13%	1-38%	0-98%		KRS motif of the NADP(H) binding pocket; disrupted nucleotide binding	[27]
R1000	R425K	0-13%	1-38%	0-98%		KRS motif of the NADP(H) binding pocket; disrupted nucleotide binding	[27]
R1000	R425C	425% or 10%	8%	12%	in isolated dIII, fully in apo form	KRS motif of the NADP(H) binding pocket; disrupted nucleotide binding	[37,39]
G1005	G430C	850%	N/A	14%	in isolated dIII, 65% with NADPH, 32% in apo form; forward reaction rate increased ~300 fold; 110x faster NADPH release	part of the E loop important for stabilisation of the occluded state; nucleotide exchange can proceed without dII-dIII interaction, hence decoupled phenotype and accelerated reverse reaction	[39,40]
Y1006	Y431C	450%	16%	N/A	in isolated dIII; forward reaction rate increased 100-fold; 5x faster NADPH release	part of the E loop important for stabilisation of the occluded state; nucleotide exchange can proceed without dII-dIII interaction, hence decoupled phenotype and accelerated reverse reaction	[40]
Y1006	Y431H	~3%	N/A	11%	In full NNT	part of the E loop important for stabilisation of the occluded state	[16]
Y1006	Y431L	6%	N/A	8%	In full NNT	part of the E loop important for stabilisation of the occluded state	[16]
Y1006	Y431F	60-80%	N/A	19-113%	pumps protons; ~3x increase for $APAD^+$	part of the E loop important for stabilisation of the occluded state	[16]
Y1006	Y431N	4%	N/A	N/A		part of the E loop important for stabilisation of the occluded state	[16]
Y1006	Y431I	4%	N/A	N/A		part of the E loop important for stabilisation of the occluded state	[16]
Y1006	double Y431F Y315F	62%	N/A	N/A		part of the E loop important for stabilisation of the occluded state	[16]
Y1006	triple alphaY226F βY315 T431	50%	N/A	N/A	increased K_m for both substrates	part of the E loop important for stabilisation of the occluded state	[16]
A1007	A432C	150%	N/A	63%	in isolated dIII, 78% with NADPH, 22% in apo form; forward reaction rate increased 3-fold	part of the E loop important for stabilisation of the occluded state	[39,40]
K1027	K452D	4-44%	8-39%	0-99%		surface-exposed residue, not part of catalytic machinery	[27]
K1027	K452G	4-44%	8-39%	0-99%		surface-exposed residue, not part of catalytic machinery	[27]
A1035	K460Q	57%	61%	N/A			[41]

K1036	A461C	46%	57%	N/A		[41]
K1036	A461F	42%	70%	N/A		[41]
K1036	A461P	48%	59%	N/A		[41]
K1036	A461R	86%	118%	N/A		[41]
K1036	A461S	69%	93%	N/A		[41]
K1036	A461L	68%	86%	N/A		[41]
V1037	L462A	38%	55%	N/A		[41]
V1037	L462E	47%	70%	N/A		[41]
V1037	L462G	58%	86%	N/A		[41]
V1037	L462P	37%	52%	N/A		[41]
V1037	L462R	37%	45%	N/A		[41]
V1037	L462T	62%	102%	N/A		[41]
V1037	delta462	28%	27%	N/A		[41]
V1037	delta461-462	3%	2%	N/A	~50% incorporation into membrane	[41]
V1037	delta460-462	1%	0%	N/A	not even incorporated into membrane	[41]
V1037	delta456-462	1%	1%	N/A	not even incorporated into membrane	[41]
V1037	delta448-462	1%	1%	N/A	not even incorporated into membrane	[41]
V1037	delta442-462	8%	7%	N/A	not even incorporated into membrane	[41]
V1037	delta431-462	1%	0%	N/A	not even incorporated into membrane	[41]

Supplementary Table 2. Catalytic activities of site-directed mutants in *R. rubrum* NNT

Homol-ogous ovine residue	*R. rubrum* mutation	Reverse activity	Cyclic activity	Proton pumping activity	Notes	Structural and mechanistic explanation if conserved	Reference
V16	I3A	69%	100%	N/A	K_d for NADH unchanged		[42]
I108	M97A	62%	98%	N/A	K_d for NADH unchanged		[42]
I108	M97L	66%	91%	N/A	K_d for NADH unchanged		[42]
I108	M97V	72%	112%	N/A	K_d for NADH unchanged		[42]
R139	R127A	0%	N/A	N/A	K_m for NADH increases from 18 to 700-800 μM; binding of NAD^+ slightly weaker; E. coli R139 changes conformation between NAD^+ and NADH bound forms	part of the NAD(H)-binding pocket, significantly changes conformation between NAD^+, NADH and apo states as demonstrated in *E. coli* NNT; no NADH binding leads to complete inhibition	[43]
R139	R127M	0%	N/A	N/A	K_m for NADH increases from 18 to 700-800 μM; binding of NAD^+ only slightly weaker; E. coli R139 changes conformation between NAD^+ and NADH bound forms	part of the NAD(H)-binding pocket, significantly changes conformation between NAD^+, NADH and apo states as demonstrated in *E. coli* NNT; no NADH binding leads to complete inhibition	[43]
Q144	Q132N	0%	0%	N/A	hydride transfer abolished but still binds NAD(H) with approximately the same affinity	important for stabilising nicotinamide ring of NAD(H) during hydride transfer; hence complete inhibition of activities	[43,44]
D147	D135N	0%	0%	N/A	no effect on K_m of NAD(H)	immediate vicinity to the NAD(H) binding site and R139; complete inhibition suggests a role in stabilising an intermediate state	[43]
S150	S138A	0%	N/A	N/A	no effect on K_m of NAD(H)	immediate vicinity to the NAD(H) binding site and R139; complete inhibition suggests a role in stabilising an intermediate state	[43]
Y158	Y146A	<10%	N/A	N/A	Weaker NADH binding, purifies as a monomer	part of the dI-dI interface; strong inhibition of activity suggests that working as a dimer in anti-phase fashion is essential	[45]
Y158	Y146F	80%	N/A	N/A		part of the dI-dI interface; only slight inhibition as dI can still dimerise	[45]
none	M226F	55%	35%	N/A	K_d of NADH increases from 30 μM to 130 μM, forward reaction inhibited slightly (~30%)		[46]
G241	T231C	58%	90%	N/A	K_d of NADH increases from 30 μM to 58 μM, forward reaction inhibited slightly (~30%)		[46]
G244	G234A	51%	15%	N/A	K_d of NADH increases from 30 μM to 33-35 μM, forward reaction inhibited slightly (~30%)	part of the NAD(H)-binding pocket and the mobile loop; slight inhibition of activities due to weaker NAD(H) binding	[46]
Y245	Y235N	~20%	2-3%	N/A	forward reaction inhibited by ~50%; however, reverse and forward reactions are rate-limited by product release from dIII and cyclic is rate-limited by hydride transfer	part of the NAD(H)-binding pocket and the mobile loop; almost complete inhibition of cyclic reaction, Y235 essential for stabilisation of the intermediate during hydride transfer	[47,48]
Y245	Y235F	~50%	7-8%	N/A	forward reaction inhibited by ~50%; however, reverse and forward reactions are rate-limited by product release from dIII and cylic is rate-limited by hydride transfer	part of the NAD(H)-binding pocket and the mobile loop; almost complete inhibition of cyclic reaction, Y235 essential for stabilisation of the intermediate during hydride transfer	[47,48]
A246	A236G	72%	53%	N/A	K_d of NADH increases from 30 μM to 300-400 μM, forward reaction inhibited slightly (~30%)	part of the NAD(H)-binding pocket and the mobile loop; slight inhibition due to weaker NAD(H) binding	[46]
K247	K237M	75%	63%	N/A	K_d of NADH increases from 30 μM to 75-85 μM, forward reaction inhibited slightly (~40%)	part of the NAD(H)-binding pocket and the mobile loop; slight inhibition due to weaker NAD(H) binding	[46]
M258	M239I	80%	30%	N/A	K_m for NADH increased ~3-fold	not part of catalytic machinery	[49]
M258	M239F	58%	16%	N/A	K_m for NADH increased ~3-fold	not part of catalytic machinery	[49]
L353	L343V	69%	95%	N/A	K_d for NADH unchanged	buried residue	[42]

Supplementary Table 3: Missense mutations in human patients with familial glucocorticoid deficiency

Homol-ogous ovine residue	*Human* mutation	Reverse activity	Cyclic activity	Proton pumping activity	Notes	Structural and mechanistic explanation if conserved	Reference
S150	S150N	N/A	N/A	N/A		immediate vicinity of the NAD(H) binding pocket	[50]
G157	G157S	N/A	N/A	N/A	more severe phenotype, includes mineralocorticoid deficiency	immediate vicinity of the NAD(H) binding pocket	[51]
F172	F172S	N/A	N/A	N/A		part of the dI-dI interface	[52]
M294	M294V	N/A	N/A	N/A		buried residue	[53]
T314	T314A	N/A	N/A	N/A		buried residue	[50]
Y345	Y345S	N/A	N/A	N/A		buried residue, relatively close to the dI-dI interface	[54]
P394	P394L	N/A	N/A	N/A		surface exposed residue, immediate vicinity to the dI-dII linker	[50,53]
A490	A490V	N/A	N/A	N/A		immediate vicinity to the proton translocation pathway	[50]
G621	G621R	N/A	N/A	N/A		buried residue	[50]
G635	G635R	N/A	N/A	N/A		membrane-facing residue	[50]
G819	G819D	N/A	N/A	N/A		close vicinity to the proton translocation pathway	[50]
A820	A820E	N/A	N/A	N/A	More severe phenotype with hypoglycaemia and precocious puberty	close vicinity to the proton translocation pathway	[53]
L934	L934P	N/A	N/A	N/A		part of the conserved helix 4 important for dII-dIII interface formation	[50]
A965	A965P	N/A	N/A	N/A		forms the NADP(H)-binding pocket	[50]
N966	N966K	N/A	N/A	N/A		forms the NADP(H)-binding pocket	

References

1. Leung, J. H. *et al.* Structural biology. Division of labor in transhydrogenase by alternating proton translocation and hydride transfer. *Science* **347**, 178–81 (2015).
2. Padayatti, P. S. *et al.* Critical Role of Water Molecules in Proton Translocation by the Membrane-Bound Transhydrogenase. *Structure* 1–9 (2017).
3. Yamaguchi, M., Wakabayashi, S. & Hatefi, Y. Mitochondrial Energy-Linked Nicotinamide Nucleotide Transhydrogenase: Effect of Substrates on the Sensitivity of the Enzyme to Trypsin and Identification of Tryptic Cleavage Sites. *Biochemistry* **29**, 4136–4143 (1990).
4. Venning, J. D., Peake, S. J., Quirk, P. G. & Jackson, J. B. Stopped-flow reaction kinetics of recombinant components of proton-translocating transhydrogenase with physiological nucleotides. *J. Biol. Chem.* **275**, 19490–7 (2000).
5. Venning, J. D., Bizouarn, T., Cotton, N. P. J., Quirk, P. G. & Jackson, J. B. Stopped-flow kinetics of hydride transfer between nucleotides by recombinant domains of proton-translocating transhydrogenase. *Eur. J. Biochem.* **257**, 202–209 (1998).
6. Hutton, M., Day, J. M., Bizouarn, T. & Jackson, J. B. Kinetic resolution of the reaction catalysed by proton-translocating transhydrogenase from Escherichia coli as revealed by experiments with analogues of the nucleotide substrates. *Eur. J. Biochem.* **219**, 1041–1051 (1994).
7. Cotton, N. P. J., White, S. A., Peake, S. J., Mcsweeney, S. & Jackson, J. B. The Crystal Structure of an Asymmetric Complex of the Two Nucleotide Binding Components of Proton-Translocating Transhydrogenase. *Structure* **9**, 165–176 (2001).
8. Sundaresan, V., Chartron, J., Yamaguchi, M. & Stout, C. D. Conformational Diversity in NAD(H) and Interacting Transhydrogenase Nicotinamide Nucleotide Binding Domains. *J. Mol. Biol.* **346**, 617–629 (2005).
9. Singh, A. *et al.* Interactions between transhydrogenase and thio-nicotinamide analogues of NAD(H) and NADP(H) underline the importance of nucleotide conformational changes in coupling to proton translocation. *J. Biol. Chem.* **278**, 33208–33216 (2003).
10. Mather, O. C., Singh, A., Van Boxel, G. I., White, S. A. & Jackson, J. B. Active-site conformational changes associated with hydride transfer in proton-translocating transhydrogenase. *Biochemistry* **43**, 10952–10964 (2004).
11. Cooley, R. B., Arp, D. J. & Karplus, P. A. Evolutionary Origin of a Secondary Structure: π-Helices as Cryptic but Widespread Insertional Variations of α-Helices That Enhance Protein Functionality. *J. Mol. Biol.* **404**, 232–246 (2010).
12. Efremov, R. G. & Sazanov, L. A. Structure of the membrane domain of respiratory complex i. *Nature* **476**, 414–421 (2011).
13. Prasad, G. S. *et al.* Crystal structures of transhydrogenase domain I with and without bound NADH. *Biochemistry* **41**, 12745–12754 (2002).
14. Johansson, T. *et al.* X-ray structure of domain I of the proton-pumping membrane protein transhydrogenase from Escherichia coli. *J. Mol. Biol.* **352**, 299–312 (2005).
15. Hu, X., Zhang, J. & Rydström, J. Interactions of reduced and oxidized nicotinamide mononucleotide with wild-type and αD195E mutant proton-pumping nicotinamide nucleotide transhydrogenases from Escherichia coli. *Biochim. Biophys. Acta* -

Bioenerg. **1367**, 134–138 (1998).

16. Olausson, T. *et al.* Site-directed mutagenesis of tyrosine residues at nicotinamide nucleotide binding sites of Escherichia coli transhydrogenase. *Biochemistry* **32**, 13237–13244 (1993).
17. Glavas, N., Ahmad, S., Bragg, P. D., Olausson, T. & Rydström, J. Identification of N,N'-dicyclohexylcarbodiimide-reactive glutamic and aspartic acid residues in Escherichia coli transhydrogenase and the exchange of these by site-specific mutagenesis. *J. Biol. Chem.* **268**, 14125–30 (1993).
18. Meuller, J. & Rydström, J. The membrane topology of proton-pumping Escherichia coli transhydrogenase determined by cysteine labeling. *J. Biol. Chem.* **274**, 19072–19080 (1999).
19. Bragg, P. D. & Hou, C. Mutation of conserved polar residues in the transmembrane domain of the proton-pumping pyridine nucleotide transhydrogenase of Escherichia coli. *Arch Biochem Biophys* **363**, 182–190 (1999).
20. Holmberg, E. *et al.* Prediction and site-specific mutagenesis of residues in transmembrane alpha-helices of proton-pumping nicotinamide nucleotide transhydrogenases from Escherichia coli and bovine heart mitochondria. *Biochemistry* **33**, 7691–700 (1994).
21. Bragg, P. D. & Hou, C. The Role of Conserved Histidine Residues in the Pyridine Nucleotide Transhydrogenase of Escherichia Coli. *Eur. J. Biochem.* **241**, 611–618 (1996).
22. Althage, M. *et al.* Cross-linking of transmembrane helices in proton-translocating nicotinamide nucleotide transhydrogenase from Escherichia coli: implications for the structure and function of the membrane domain. *Biochim. Biophys. Acta - Bioenerg.* **1659**, 73–82 (2004).
23. Glavas, N. A. & Bragg, P. D. The mechanism of hydride transfer between NADH and 3-acetylpyridine adenine dinucleotide by the pyridine nucleotide transhydrogenase of Escherichia coli. *Biochim. Biophys. Acta* **1231**, 297–303 (1995).
24. Yamaguchi, M., Stout, D. C. & Hatefi, Y. The proton channel of the energy-transducing nicotinamide nucleotide transhydrogenase of Escherichia coli. *J. Biol. Chem.* **277**, 33670–33675 (2002).
25. Glavas, N. A., Hou, C. & Bragg, P. D. Involvement of Histidine-91 of the β Subunit in Proton Translocation by the Pyridine Nucleotide Transhydrogenase of Escherichia coli. *Biochemistry* **34**, 7694–7702 (1995).
26. Bragg, P. D. & Hou, C. Characterization of mutants of βHistidine91, βAspartate213, and βAsparagine222, possible components of the energy transduction pathway of the proton-translocating pyridine nucleotide transhydrogenase of Escherichia coli. *Arch. Biochem. Biophys.* **388**, 299–307 (2001).
27. Hu, X., Zhang, J., Fjellström, O., Bizouarn, T. & Rydström, J. Site-directed mutagenesis of charged and potentially proton-carrying residues in the β subunit of the proton-translocating nicotinamide nucleotide transhydrogenase from escherichia coli. Characterization of the βH91, βD392, and βK424 mutants. *Biochemistry* **38**, 1652–1658 (1999).
28. Yamaguchi, M. & Stout, C. D. Essential Glycine in the Proton Channel of Escherichia coli Transhydrogenase. *J. Biol. Chem.* **278**, 45333–45339 (2003).

29. Althage, M. *et al.* Functional split and crosslinking of the membrane domain of the β subunit of proton-translocating transhydrogenase from Escherichia coli. *Biochemistry* **42**, 10998–11003 (2003).

30. Yamaguchi, M. & Hatefi, Y. Proton-translocating nicotinamide nucleotide transhydrogenase of Escherichia coli. Involvement of aspartate 213 in the membrane-intercalating domain of the beta subunit in energy transduction. *J. Biol. Chem.* **270**, 16653–16659 (1995).

31. Bragg, P. D. & Hou, C. Mutation of conserved polar residues in the transmembrane domain of the proton-pumping pyridine nucleotide transhydrogenase of Escherichia coli. *Arch Biochem Biophys* **363**, 182–190 (1999).

32. Karlsson, J., Althage, M. & Rydström, J. Roles of individual amino acids in helix 14 of the membrane domain of proton-translocating transhydrogenase from Escherichia coli as deduced from cysteine mutagenesis. *Biochemistry* **42**, 6575–6581 (2003).

33. Althage, M., Bizouarn, T. & Rydström, J. Identification of a region involved in the communication between the NADP(H) binding domain and the membrane domain in proton pumping E. coli transhydrogenase. *Biochemistry* **40**, 9968–9976 (2001).

34. Bragg, P. D., Glavas, N. A. & Hou, C. Mutation of Conserved Residues in the NADP(H)-Binding Domain of the Proton Translocating Pyridine Nucleotide Transhydrogenase ofEscherichia coli. *Arch. Biochem. Biophys.* **338**, 57–66 (1997).

35. Ahmad, S., Glavas, N. A. & Bragg, P. D. A mutation at Gly314 of the β subunit of the Escherichia coli pyridine nucleotide transhydrogenase abolishes activity and affects the NADP(H)-induced conformational change. *Eur. J. Biochem.* **207**, 733–739 (1992).

36. Johansson, C., Bergkvist, A., Fjellström, O., Rydström, J. & Karlsson, B. G. Sequential assignment and secondary structure analysis of the NADP(H)-binding domain of Escherichia coli transhydrogenase. *J. Biomol. NMR* **14**, 295–6 (1999).

37. Fjellström, O. *et al.* Mapping of residues in the NADP(H)-binding site of proton-translocating nicotinamide nucleotide transhydrogenase from Escherichia coli. A study of structure and function. *J. Biol. Chem.* **274**, 6350–6359 (1999).

38. Meuller, J., Hu, X., Bunthof, C., Olausson, T. & Rydström, J. Identification of an aspartic acid residue in the β subunit which is essential for catalysis and proton pumping by transhydrogenase from Escherichia coli. *Biochim. Biophys. Acta - Bioenerg.* **1273**, 191–194 (1996).

39. Bergkvist, A., Johansson, C., Johansson, T., Rydstrom, J. & Karlsson, B. G. Interactions of the NADP(H)-binding domain III of proton-translocating transhydrogenase from Escherichia coli with NADP(H) and the NAD(H)-binding domain I studied by NMR and site-directed mutagenesis. *Biochemistry* **39**, 12595–12605 (2000).

40. Johansson, C., Pedersen, A., Karlsson, B. G. & Rydström, J. Redox-sensitive loops D and E regulate NADP(H) binding in domain III and domain I-domain III interactions in proton-translocating Escherichia coli transhydrogenase. *Eur. J. Biochem.* **269**, 4505–4515 (2002).

41. Bragg, P. D. & Hou, C. Effect of truncation and mutation of the carboxyl-terminal region of the β subunit on membrane assembly and activity of the pyridine nucleotide transhydrogenase of Escherichia coli. *Biochim. Biophys. Acta - Bioenerg.* **1365**, 464–472 (1998).

42. Tveen Jensen, K., Strambini, G., Gonnelli, M., Broos, J. & Jackson, J. B. Mutations in Transhydrogenase Change the Fluorescence Emission State of TRP72 from 1La to 1Lb. *Biophys. J.* **95**, 3419–3428 (2008).

43. Brondijk, T. H. C. *et al.* The role of invariant amino acid residues at the hydride transfer site of proton-translocating transhydrogenase. *J. Biol. Chem.* **281**, 13345–13354 (2006).

44. Van Boxel, G. I., Quirk, P. G., Cotton, N. P. J., White, S. A. & Jackson, J. B. Glutamine 132 in the NAD(H)-binding component of proton-translocating transhydrogenase tethers the nucleotides before hydride transfer. *Biochemistry* **42**, 1217–1226 (2003).

45. Obiozo, U. M. *et al.* Substitution of tyrosine 146 in the dI component of proton-translocating transhydrogenase leads to reversible dissociation of the active dimer into inactive monomers. *J. Biol. Chem.* **282**, 36434–36443 (2007).

46. Gupta, S. *et al.* Mutation of amino acid residues in the mobile loop region of the NAD(H)-binding domain of proton-translocating transhydrogenase. *Biochim. Biophys. Acta - Bioenerg.* **1409**, 25–38 (1998).

47. Diggle, C. *et al.* Mutation of Tyr235 in the NAD(H)-binding subunit of the proton-translocating nicotinamide nucleotide transhydrogenase of Rhodospirillum rubrum affects the conformational dynamics of a mobile loop and lowers the catalytic activity of the enzyme. *J. Biol. Chem.* **271**, 10109–15 (1996).

48. Bizouarn, T., Grimley, R., Diggle, C., Thomas, C. M. & Jackson, J. B. Mutations at tyrosine-235 in the mobile loop region of domain I protein of transhydrogenase from Rhodospirillum rubrum strongly inhibit hydride transfer. *Biochim. Biophys. Acta - Bioenerg.* **1320**, 265–274 (1997).

49. Grimley, R. L., Quirk, P. G., Bizouarn, T., Thomas, C. M. & Jackson, J. B. Role of methionine-239, an amino acid residue in the mobile-loop region of the NADH-binding domain (domain I) of proton-translocating transhydrogenase. *Biochemistry* **36**, 14762–14770 (1997).

50. Meimaridou, E. *et al.* Mutations in NNT encoding nicotinamide nucleotide transhydrogenase cause familial glucocorticoid deficiency. *Nat. Genet.* **44**, 740–2 (2012).

51. Weinberg-Shukron, A. *et al.* Combined mineralocorticoid and glucocorticoid deficiency is caused by a novel founder nicotinamide nucleotide transhydrogenase mutation that alters mitochondrial morphology and increases oxidative stress. *J. Med. Genet.* **52**, 636–641 (2015).

52. Yamaguchi, R. *et al.* A novel homozygous mutation of the nicotinamide nucleotide transhydrogenase gene in a Japanese patient with familial glucocorticoid deficiency. *Endocr. J.* **60**, 855–859 (2013).

53. Roucher-Boulez, F. *et al.* NNT mutations: a cause of primary adrenal insufficiency, oxidative stress and extra- adrenal defects. *Eur. J. Endocrinol.* **175**, 73–84 (2016).

54. Hershkovitz, E., Arafat, M., Loewenthal, N., Haim, A. & Parvari, R. Combined adrenal failure and testicular adrenal rest tumor in a patient with nicotinamide nucleotide transhydrogenase deficiency. *J. Pediatr. Endocrinol. Metab.* **28**, 1187–90 (2015).